MRTF promotes breast cancer cell motility through SRF-dependent upregulation of *DIAPH3* expression

Ian Eder[1], Virginia Yu[1], Fangyuan Chen[2,3], David Gau[1], Marion Joy[4],

Peter Lucas[5], David Boone[6], Adrian V. Lee[7], Partha Roy[1,5]

[1]Bioengineering, University of Pittsburgh
[2]School of Medicine, University of Pittsburgh
[3]School of Medicine, Tsinghua University, China
[4] Hillman Cancer Center, University of Pittsburgh
[5]Pathology, University of Pittsburgh
[6]Biomedical Informatics, University of Pittsburgh
[7]Pharmacology, University of Pittsburgh

Corresponding author:
Partha Roy, Ph.D, 306 CNBIO, 300 Technology Drive, University of Pittsburgh, Pittsburgh, PA 15219, USA; Tel: 1-412-624-7867; Fax: 412-383-8788; Email: par19@pitt.edu

Running title: MRTF-dependent control of cell migration by DIAPH3

ABSTRACT

Dysregulated actin cytoskeleton gives rise to aberrant cell motility and metastatic spread of tumor cells. The MRTF-SRF transcriptional complex plays a key role in regulating the expressions of actin cytoskeleton-modulatory genes. In this study, we demonstrate that MRTF's interaction with SRF is critical for migration and invasion of breast cancer cells. Disruption of the MRTF-SRF interaction suppresses membrane dynamics affecting the frequency and the effectiveness of membrane protrusion during cell motility. Consistent with these phenotypic changes, we further show that MRTF promotes actin polymerization at the leading edge, a key aspect of membrane protrusion, and migration of breast cancer cells through upregulating the expression of formin-family actin nucleating/elongating protein encoding gene *DIAPH3* in an SRF-dependent manner. In support of these findings, multiplexed quantitative immunohistochemistry and transcriptome analyses of clinical specimens of breast cancer further demonstrate a positive correlation between nuclear localization of MRTF with malignant traits of cancer cells as well as enrichment of MRTF/SRF gene signature in distant metastases relative to primary tumors. In conclusion, this study for the first time links the MRTF/SRF signaling axis to cell migration through the regulation of a specific actin-binding protein, and provides evidence for an association between MRTF/SRF activity and malignancy in human breast cancer.

Keywords: MRTF, actin, SRF, breast cancer, cell motility, diaphanous

INTRODUCTION

The vast majority of breast cancer (BC)-related deaths are due to the metastatic spread of tumor cells to distant organs. Metastasis is a complex process consisting of multiple steps, including tumor cell invasion through the stromal tissue followed by intravasation, extravasation, and ultimately colonization of tumor cells at the distant organ site. The initial step in this cascade of events, stromal invasion of cancer cells, is highly dependent upon dynamic actin remodeling in tumor cells and the action of various secreted ECM-degrading proteases. Disruption of actin cytoskeleton homeostasis is a critical feature of metastatic cancer cells. In principle, restoration of actin cytoskeleton normality should attenuate migratory propensity of tumor cells reducing metastatic burden in breast cancer patients.

Myocardin-related Transcription Factor (MRTF), a family of transcriptional co-activators, is a major regulator of the expression of genes relevant to cytoskeleton organization, cell adhesion and ECM remodeling [summarized in (Gau and Roy, 2018). There are two isoforms of MRTF in non-muscle cells: MRTF-A (also known as MKL1 or MAL), and MRTFB (also known as MKL2). Both isoforms of MRTF share common structural motifs. At the N-terminus, they contain three RPEL domains which in addition to the space regions bind G-actin in a pentavalent G-actin-MRTFA Complex (Mouilleron et al., 2011). Interspersed in the last two RPEL domains, there is a bi-partite basic-rich region (B2-B3) containing a nuclear localization signal (NLS) which becomes exposed once G-actin is unbound (Mouilleron et al., 2011, Nakamura et al., 2010, Pawlowski et al., 2010). The other conserved domains are a basic-rich B1 domain (contains a second NLS and SRF-binding region), a glutamine-rich Q domain (promotes nuclear export), a SAP domain (a putative chromatin-binding domain), a leucine-zipper domain (mediates homo- and hetero-dimerization), a PPxY domain (mediates interactions with WW domains of partner proteins including YAP), and a C-terminal transcriptional activation domain (Miralles et al., 2003, Mouilleron et al., 2011).

MRTF operates to regulate gene expression through two distinct mechanisms. First, when activated upon growth factor stimulation it directly binds to and acts as a transcriptional co-factor of serum response factor (SRF) orchestrating a broad transcriptional program including expression of SRF itself and many

other genes, a subset of which are relevant for actin cytoskeletal control (Gualdrini et al., 2016). Notably, MRTF preferentially interacts with SRF as a dimer rather a monomer (Miralles et al., 2003). Second, MRTF can directly bind to DNA through its SAP domain to promote gene expression in an SRF-independent manner (Gurbuz et al., 2014, Asparuhova et al., 2015). MRTF is a highly regulated transcription factor. In resting cells, binding to G-actin sequesters MRTF in the cytoplasmic compartment restricting its transcriptional activity. Induction of actin polymerization liberates MRTF from G-actin, allowing MRTF to translocate to the nucleus and participate in gene regulatory activities. Therefore, nuclear translocation and transcriptional activity of MRTF are highly sensitive to the relative abundance of G- and F-actin in cells (Miralles et al., 2003, Posern et al., 2004, Vartiainen et al., 2007).

A number of previous studies have demonstrated that loss of expression of either MRTFs or SRF causes defects in actin cytoskeleton and cell migration in physiological and pathological contexts (summarized in (Gau and Roy, 2018)). However, since MRTF has SRF-independent gene regulatory activities, and conversely, SRF is also activated by Ternary Complex Factor (TCF) family of transcriptional cofactors leading to gene expression program that is distinct from ones triggered by activated MRTF-SRF complex, the precise role of MRTF-SRF interaction in cell migration cannot be extrapolated from those loss-of-function studies. In this study, we for the first time directly demonstrate the critical importance of MRTF-SRF interaction in cell migration and invasion, link upregulation of formin-family actin-binding protein (ABP) diaphanous-related formin 3 (*DIAPH3* - encodes mDia2) expression as a key mechanism of MRTF-directed control of cell migration, and further provide clinical evidence for MRTF activity association with increased malignancy in human BC.

RESULTS

MRTF-SRF interaction is critical for migration and invasion of breast cancer cells

To investigate the role of MRTF-SRF interaction in breast cancer cell motility, we performed cell migration studies using MDA-MB-231 (MDA-231), a widely used metastatic human triple-negative breast cancer (TNBC - lacks the expression of estrogen receptor (ER), progesterone receptor (PR) and HER2 receptor) cell line as a model system, in an overexpression-based experimental setting. A previous study found that stable co-silencing of MRTF isoforms led to reduced migration and invasion of MDA-231 cells *in vitro* and *in vivo* (Medjkane et al., 2009), a trend that is also recapitulated when MRTF isoforms are partially depleted acutely in an siRNA transfection setting (**Fig S1**). These findings demonstrate MRTF-dependence for motility of MDA-231 cells therefore justifying its use as a model cell line for the purpose of our studies. In our overexpression studies, we utilized our previously generated GFP/luciferase (Luc) expressing sublines of MDA-231 cells engineered for doxycycline (dox)-inducible stable overexpression of either wild-type MRTF-A (WT-MRTF-A) or a SAP-domain deleted mutant form of MRTF-A (referred to as ΔSAP-MRTF-A hereon) or a SRF-binding-deficient point-mutant of MRTF-A (referred to as ΔSRF-MRTF-A hereon) (Gau et al., 2022). **Fig 1A** depicts the mutations performed to generate the ΔSRF-MRTF-A and ΔSAP-MRTF-A constructs. A dox-treated GFP/luciferase-expressing subline without any additional MRTF-A perturbation served as the control. Although the expression levels of mCherry (which is co-expressed with the various MRTF-A constructs under the same dox-inducible promoter in an IRES system) are similar between the sublines, interestingly, the total protein abundance of MRTF-A in ΔSRF-MRTF-A overexpressing cells, while higher than that of control cells, was demonstrably lower than both WT- and ΔSAP-MRTF-A overexpressing sublines (**Fig 1B**). As per RNA-sequencing data (discussed later), MRTF-A mRNA expression was also relatively comparable across the various MRTF-A overexpressing cell lines (**Fig S2**). Therefore, it is unlikely that MRTF-A expression is transcriptionally augmented in a positive feedback manner when either WT- or ΔSAP-MRTF-A is exogenously overexpressed, and this is blocked when SRF's interaction is disrupted in our cell lines. However, it is possible that disrupting SRF's interaction of MRTF-A may somehow either impact the protein translation and/or the rate of protein turnover of MRTF-A.

We first performed time-lapse single-cell imaging of 2D random motility of the various dox-inducible MRTF-A overexpressing MDA-231 sublines, with transgene overexpression turned on 48h prior to time-lapse imaging. **Fig 1C** shows the trajectories of individual groups of cells obtained from 3-hour time-lapse recordings (pooled from three independent experiments). As summarized in **Fig 1D**, overexpression of WT-MRTF-A accelerated cell migration by ~30% relative to control cells in a statistically significant manner. Although overexpression of ΔSAP-MRTF-A resulted in a marginal 15% increase in average migration speed relative to control cells, this difference was not statistically significant. The most striking feature from these experiments is a robust 54% decrease in the speed of migration exhibited by the ΔSRF-MRTF-A overexpressing cells when compared to control cells. Although ΔSRF-MRTF-A expressers have lower level of MRTF-A than the other two MRTF-A overexpressing sublines, we do not think the motility phenotype of ΔSRF-MRTF-A expressers is simply caused by the differences in MRTF-A protein level between the sublines. This is because ΔSRF-MRTF-A expressers exhibit substantially reduced motility despite having higher level of MRTF-A than control cells, a result that can be potentially explained by a dominant negative action of this mutant (this is highly probable because MRTFs homo- as well as hetero-dimerize and preferentially bind to SRF in a dimerized form). We also analyzed the effect of overexpression of these MRTF-A variants on the persistence of cell migration. To represent this metric, we computed the standard deviation of the change in migration direction ($\Delta\theta$) every 30 minutes. A higher standard deviation of $\Delta\theta$ indicates a greater fluctuation in the direction of cell migration. While the values of standard deviation of $\Delta\theta$ were not statistically different between control, WT-MRTF-A, and ΔSAP-MRTF-A expressers, overexpression of ΔSRF-MRTF-A reduced the standard deviation of $\Delta\theta$ relative to control (by ~25%) as well as the other two sublines in a statistically significant manner (**Fig 1E**). These data suggest that disruption of the MRTF-SRF interaction decreases the speed but improves the persistence of cell migration and underscore a critical importance of the MRTF-SRF interaction for efficient motility of breast cancer cells.

To better represent the *in vivo* scenario of stromal invasion of cancer cells from a tumor, we next performed tumor spheroid invasion assays in collagen-I matrix over a period of 96 hours. Since we apriori found that induction of ΔSRF-MRTF-A expression inhibits tumor spheroid formation, dox-induced transgene expression for all experimental groups was turned on only after the spheroid formation was complete. Representative images of tumor spheroids for different groups at the 0- and 96-hour time-points (by either phase-contrast imaging or fluorescence imaging of DAPI/phalloidin-stained cells) are shown in **Fig 2A**. To quantify the directed invasion of tumor spheroids, we normalized the end-point DAPI positive area to the initial spheroid area (assessed from the phase-contrast images). Consistent with our 2D migration data, collagen invasiveness of tumor spheroids was also strikingly inhibited (by 54%) upon disruption of the MRTF-SRF interaction compared to WT MRTF-A overexpressing cells (**Fig 2B**) further underscoring the critical importance of MRTF-SRF interaction for ECM invasion. However, contrasting our 2D migration data, overexpression of either WT- or ΔSRF-MRTF-A also reduced invasion of MDA-231 tumor spheroids but clearly not to the same extent as elicited by overexpression of ΔSRF-MRTF-A, suggesting that excessively high MRTF activity may be somewhat counterproductive for tumor cell invasion. Possible reasons underlying the differential effect of WT MRTF-A overexpression on 2D random motility *vs* 3D invasion collagen invasion are discussed later.

Disruption of the MRTF-SRF interaction affects membrane protrusion

Since lamellipodial protrusion is the initiating step for cell migration, to further understand the physical basis for the defect in cell migration induced by the disruption of MRTF-SRF binding, we comparatively analyzed the leading edge dynamics between the various groups of cells by performing kymography analyses. From the representative kymography scans of the various sublines of MDA-231 cells (shown in **Fig 3A**), it was qualitatively obvious that unlike the other three sublines, ΔSRF-MRTF-A expressers exhibited much less fluctuation of the membrane (marked by cycles of protrusions and retraction)

suggesting that membrane dynamics is suppressed as a result of the inhibition of the MRTF-SRF interaction. In order to quantitatively describe these changes, we used an automated image analysis pipeline to detect local minimum and maximum in the protruding membrane at the leading edge. Based on these analyses, we quantified three parameters including the frequency of protrusion, net protrusion distance (i.e. equal to the protrusion distance minus the retraction distance) and the duration of protrusion ascent (i.e. the time taken for the protrusion to go from the local minimum to the local maximum). Although overexpression of WT-MRTF-A slightly reduced the frequency of protrusion relative to control (**Fig 3B**), the net protrusion distance and the duration of protrusion ascent, features that are indicative of productive protrusions and increase the efficiency of cell migration, were both found to be augmented upon elevated MRTF-A expression (**Figs 3C and 3D**). Disruption of the SAP-domain interaction of MRTF-A did not reverse MRTF-A-induced increase in net protrusion distance and duration of protrusion ascent. However, inhibition of SRF's interaction of MRTF-A not only resulted in reduced protrusion frequency (lowest among the four groups) but also blocked MRTF-A-induced increase in protrusion distance (**Figs 3B, C**). Interestingly, although protrusions were initiated much less frequently in ΔSRF-MRTF-A expressers, the average duration of protrusion ascent of these cells (18.68 ± 8.76s) was longer than that calculated for control cells (15.08 ± 7.01s), an observation that is consistent with the trend of improved persistence of motion exhibited by these cells as illustrated in **Fig 1E**. Overall, these results suggest that altered membrane protrusion dynamics is a distinguishing phenotypic consequence of the disruption of MRTF-SRF interaction in cells.

DIAPH3 is a key mediator of MRTF-A induced promotion of breast cancer cell motility

Membrane protrusion is orchestrated by the coordinated actions of a wide-range of ABPs. These ABPs include proteins involved in maintenance of monomeric actin pool via G-actin sequestering, nucleotide exchange on G-actin, nucleation and/or elongation of actin filaments, disassembly of actin filaments, filament severing, capping and crosslinking of actin filaments. Therefore, to determine which of these major classes of ABPs are transcriptionally altered upon various functional perturbations of MRTF-A, we performed bulk RNA-sequencing analyses of both 2D and 3D cultures of control vs various MRTF-A overexpressing sublines of MDA-231 cells. We then derived differentially expressed genes (DEGs) based on the absolute $\log_2$fold change (FC) >1.5 in gene expression, false-discovery rate (FDR) <0.001, and the expression level cut-off set to 0.1 TPM. Heat-maps of the DEGs between the cell lines (**Fig S3A**) and principal component analyses (PCA) (**Fig S3B**) revealed the overexpression of ΔSRF-MRTF-A had the most dramatic impact on the gene expression profile in MDA-231 cells. The transcriptional profiles of major ABPs belonging to the different functional categories in 2D and 3D cultures of each of the four sublines are shown in the form of heat-plots in **Fig 4A** and **Fig 4B**, respectively. We specifically filtered for genes which were differentially expressed (defined as greater than 2 Z-scores; Z scores were calculated using the mean and standard deviation of the control cells for each gene) between WT-MRTF-A and ΔSRF-MRTF-A overexpressers, and in the opposite directions relative to control cells (**Fig 4C**). From this list, we identified *DIAPH3* to be the only gene that was reproducibly altered at the mRNA level in a consistent direction in both 2D and 3D cultures.

Formin-family DIAPH3 (encodes mDia2) is one of the three human orthologs of drosophila *Diaphanous* (Schoen et al., 2013). Like other members of formin-family proteins, DIAPH3, when activated through its direct interaction with Rho GTPase (Rif1 specifically in the case of DIAPH3), promotes nucleation and elongation of actin filaments and formation of F-actin-based structures (Stastna et al., 2012, Gorelik et al., 2011). Although DIAPH3 is most well-known for its ability to induce filopodia formation (Schirenbeck et al., 2005, Stastna et al., 2012), overexpression of constitutively active DIAPH3 also leads to longer actin filaments in lamellipodia and improved lamellipodial protrusion in motile cells (Yang et al., 2007). Given DIAPH3's well-established role in actin polymerization and membrane protrusion, we

further investigated whether DIAPH3 could be a potential mediator of the MRTF-dependent regulation of cell migration. First, to verify MRTF-A dependent regulation of DIAPH3 expression at the protein level, we performed immunoblot analyses of MDA-231 cell lysates which showed that DIAPH3 expression is elevated upon overexpression of either WT- or ΔSAP-MRTF-A but severely downregulated when ΔSRF-MRTF-A is overexpressed **(Fig 5A)**. Consistent with these overexpression results, co-silencing of MRTF isoforms, either transiently in MDA-231 cells or stably in D2A1 (a murine breast cancer cell line) cells, downregulated DIAPH3 expression (**Fig 5B**). Collectively, these results demonstrate that MRTF-A promotes DIAPH3 expression utilizing its SRF's interaction. We also probed for changes in DIAPH1, another member of the formin family of proteins that is closely related to and has overlapping functions with DIAPH3. Although DIAPH1 expression in MDA-231 cells was not affected by either knockdown or overexpression of MRTF-A (**Fig 5B**), in D2A1 cells DIAPH1 was coordinately downregulated with DIAPH3 when MRTF expression was stably suppressed (**Fig 5C**). Therefore, it is possible that DIAPH3 is more consistently regulated by MRTF across cell lines, while MRTF's regulation of DIAPH1 expression might be cell-type specific.

Next, we analyzed 2D random migration of control and WT MRTF-A overexpressing sublines of MDA-231 with or without forced knockdown of DIAPH3; non-targeting control siRNA transfectants served as control. As expected, overexpressing WT-MRTF-A increased the average migration speed of MDA-231 cells by ~32%. Knockdown of DIAPH3 in control and MRTF-A overexpressing cells decreased average migration speed compared to their control siRNA treated counterparts by 30% and 33%, respectively, and importantly, abrogated the differences in average migration speed between the control and MRTF-A overexpressing cells (**Fig 5D;** immunoblot shown in **Fig 5E** demonstrates DIAPH3 knockdown). These results suggest that DIAPH3 upregulation is a key mechanism underlying MRTF-A-induced stimulation of cell migration.

Actin polymerization at the leading edge is a key requirement for membrane protrusion during cell migration. We previously showed that overexpression of MRTF-A increases the overall F-actin content in MDA-231 cells, a phenotype that is largely dependent on its SRF interaction (Gau et al., 2022). To further examine a potential role of DIAPH3 in MRTF-A-induced changes in actin polymerization at the leading edge, we pre-established monolayers of control and MRTF-A overexpressing cells with or without forced knockdown of DIAPH3. We then performed a wound-healing assay to induce polarized phenotype with well-defined lamellipodia in migratory cells at the edge of the wound. In parallel, we examined DIAPH3's involvement in MRTF-induced changes in global F-actin content in a culture setting that did not involve wound healing. As expected, MRTF-A overexpression conspicuously increased the overall F-content in cells marked by promotion of actin stress fibers and polymerized actin at the leading edge (**Figs 5F** and **Fig S4**). Not surprisingly, knockdown of DIAPH3 alone was not sufficient to block MRTF-A-induced increase in the overall F-actin content (**Fig S4**); however, MRTF-A-induced increase in actin polymerization at the leading edge was dramatically reversed upon DIAPH3 depletion (**Figs 5F-G**). Based on these data, we propose that DIAPH3 is a key mediator of MRTF/SRF axis-driven stimulation of actin polymerization at the leading edge and cell migration (as schematized in **Fig 5H**).

Increased MRTF activity positively correlates with local invasion and distant metastases in human breast cancer. Next, we performed multiplexed quantitative immunohistochemistry (IHC) of a human BC tissue microarray (TMA) representing 361 clinical samples (clinico-pathological features of the TMA are detailed in the "Experimental Procedures" section), staining for MRTF-A, MRTF-B, pan-cytokeratin (CK: to distinguish CK+ tumor cells from CK- stromal cells by image segmentation), and nuclear marker DAPI (representative images are shown in **Figs 6A-D**). Pan-CK staining was used to segment the TMA spots into tumor and stromal regions (the tumor masks are shown in **Figs 6B and 6E)**. Since local invasion into the stroma and/or lymph node infiltration are characteristic features of malignant cells, we performed

two metrics of analyses to query a relationship between tumor-cell intrinsic MRTF activity in an isoform-specific manner and malignancy potential of tumor cells. First, we compared the expression of each MRTF isoform between CK+ cancer cells in the bulk tumor *vs* those dispersed in the stromal region. The underlying assumption is that the latter category of cells represents locally invading cancer cells enabling their separation from the bulk tumor. Interestingly, as per these analyses, the total expression level of MRTF-A was significantly lower in cancer cells dispersed in the stroma than those in the bulk tumor (**Fig 6G**); MRTF-B expression in cancer cells was not statistically different between the two compartments (**Fig 6J**). However, when we analyzed the nuclear-to-cytoplasmic (N/C) content of each MRTF isoform (as a surrogate indicator of the transcriptionally active form of MRTF), the average N/C ratios of both MRTF-A and MRTF-B in CK+ cells were significantly higher in the stromal *vs.* the bulk tumor regions (**Figs 6H-K)**. Representative images of MRTF-A and MRTF-B nuclear localization in cancer cells in the stromal regions (marked by asterisks) and cancer cells in the bulk tumor (outlined with a dotted line) are shown in **Figs 6C and 6F**. Second, we performed correlation analyses between the N/C ratio of each MRTF isoform with the number of involved lymph nodes in the clinical specimens. When we performed these analyses including all tumor (ER+ and ER-) samples, we did not see any significant correlation between N/C ratio of either of the two MRTF isoforms and the number of lymph node involvement **(Fig S5)**. However, when these analyses were performed in a molecular subtype-specific manner, we found a significant positive correlation between the N/C ratio of MRTF-A (but not MRTF-B) and the number of lymph node involvement exclusively in lymph node positive TNBC samples (**Figs 6I, 6L**). In summary, these TMA data provided an initial indication for higher MRTF activity positively correlated with malignant traits of tumor cells in human BC, more prominently in TNBC.

Although our TMA studies utilized nuclear localization status of MRTF as a surrogate marker for the active form of MRTF, we recognize that it is still only an approximate indicator of MRTF activity. This is because the transcriptional activity of MRTF can be also regulated by nuclear actin (Miralles et al., 2003) and various post-translational modifications (Holstein et al., 2020, Panayiotou et al., 2016). Furthermore, since MRTF has both SRF-dependent/SAP-independent and SRF-independent/SAP-dependent transcriptional activities (Gurbuz et al., 2014), nuclear localization status also fails to provide any insight into different transcriptional modalities of MRTF. Therefore, we sought to investigate which specific transcriptional signature of MRTF is predominantly associated with malignancy traits in human breast cancer. Given that our TMA studies provide stronger evidence for MRTF-A's association with the malignant traits than for MRTF-B in TNBC, we overlapped DEGs between 2D cultures of control and WT MRTF-A overexpressing MDA-231 cells obtained from our studies with published DEGs of 2D cultures of MDA-231 cells in response to stable co-silencing of both MRTF isoforms restricted to identical FDR and FC criteria as previously reported by the Treisman group (Medjkane et al., 2009). From these analyses, we identified genes that were transcriptionally altered in the opposite directions in knockdown vs overexpression setting to serve as a high-stringency MRTF-A gene signature. Function-specific gene signatures were then developed by first removing DEGs which were represented in the WT- but not the corresponding functional-mutant MRTF-A overexpression setting. Then gene signature score (GSS) of downregulated genes were subtracted from GSS of upregulated genes as illustrated in the Venn diagrams (**Fig 7A**) and the table (**Fig 7B**) to generate scores which account for both positive and negative gene regulation by MRTF-A's function. Further details of the generation of the gene signature and the genes which composed these signatures can be found in the "Experimental Procedures" and **Table S1**. Next, we ran gene signature variance analyses (GSVA) using our generated gene signatures on primary breast tumors and pair-matched metastases harvested from various anatomical sites (ovary, gastrointestinal tract, brain, and bone) of BC patients (Zhu et al., 2019, Cosgrove et al., 2022). Except for bone, most metastatic sites exhibited a trend of enrichment of SRF function-specific gene signature score of MRTF-A in metastases relative to primary tumors (scores were higher in 8 out of 12 in the ovary, 4 out of 5 in the gastrointestinal (GI) tract, and 11 out of 22 in the brain) (**Fig 7C**). While site-specific analyses did not

reach statistical significance likely because of small size for each anatomical site, pooled analyses of all soft tissue metastases revealed a statistically significant enrichment of SRF function-specific but not SAP-dependent gene signature of MRTF in metastases relative to the primary tumor (**Fig 7D;**. Collectively, these data are indicative of higher MRTF/SRF activity associated with greater metastatic potential of tumor cells in human BC.

DISCUSSION

In the present study, we report several novel findings. First, while many previous studies showed defects in migration and invasion of cells in developmental and pathological (cancer) contexts upon loss of function of either MRTF or SRF by genetic or pharmacological inhibition on their own (Somogyi and Rorth, 2004, Han et al., 2004, Medjkane et al., 2009, Hayashi et al., 2014, Watanabe et al., 2015, Evelyn et al., 2010, Costello et al., 2015, Record et al., 2015, Franco et al., 2013, Weinl et al., 2013, Gau et al., 2017), to the best of our knowledge this study provides the first direct experimental evidence for a pro-migratory role of MRTF-SRF interaction in cell migration/invasion. Second, this study mechanistically links upregulation of a specific actin-binding protein (DIAPH3) to MRTF/SRF-axis dependent control of cell migration. Third, this is the first study that correlates subcellular localization of MRTF in an isoform-specific manner with the clinical features of malignancy and compares function-specific gene signature of MRTF between metastases harvested from different anatomical sites and matched primary tumors to collectively demonstrate a positive association between MRTF activity and metastatic potential of tumor cells in human BC.

Our results showing the critical importance of MRTF-SRF interaction in motility/invasion of breast cancer cells are consistent with previously reported defects in motility and invasion of breast cancer and other types of cells upon loss of either MRTF or SRF expression (Somogyi and Rorth, 2004, Han et al., 2004, Medjkane et al., 2009, Evelyn et al., 2010, Costello et al., 2015, Record et al., 2015, Franco et al., 2013, Weinl et al., 2013). However, our findings are at odds with another report that showed overexpression of ΔSRF-MRTF-A led to increased chemotactic migration of HC11 mammary epithelial cells in a transwell assay (Gurbuz et al., 2014). While the latter finding is hard to reconcile with the literature, we suspect there could be several reasons that could potentially explain the discrepancy in the results. First, a key difference is the use of cell line model – while MDA-231 cells are mesenchymal (lacks E-cadherin expression), HC11 cells are epithelial in nature where there could be a confounding factor of the effect of disruption of MRTF-SRF interaction on cell-cell interaction. Second, chemotactic migration of HC11 cells was assessed in a long-term assay (22 hr) which can have a confounding effect of cell proliferation. Third, transwell migration is also facilitated by deformability (important for cell migration through the pores) and gradient-sensing ability of cells, and it is possible that disruption of the MRTF-SRF interaction positively influences some of these aspects.

A key difference between the results of 2D migration and 3D tumor spheroid invasion experiments is the differential effect of WT MRTF-A overexpression. Contrasting its stimulatory effect on the 2D random motility in a short-term assay, overexpression of WT MRTF-A modestly reduced collagen invasiveness of MDA-231 cells in a long-term 3D tumor-spheroid invasion assay. Interestingly, we previously reported that WT MRTF-A overexpression increases the proliferation accelerating the primary tumor growth of MDA-231 cells when implanted in mice (Gau et al., 2022). Both proliferation and migration are energy-dependent processes. According to "Go-or-Grow" hypothesis, highly proliferating tumor cells undergo phenotypic switching to reduce migratory ability as a way of channeling energy utilization toward proliferation (Giese et al., 2003, Giese et al., 1996a, Giese et al., 1996b), which may partly explain the reduced invasiveness of WT MRTF-A overexpressers relative to control cells. Additionally, MMP-mediated ECM proteolysis is an important feature of tumor cell invasion, and it is possible that perturbation of MRTF can modulate the expression of certain MMPs and tissue inhibitors of MMPs

(TIMPs). Single-cell imaging of tumor cell invasion as well as imaging-based assessment of ECM proteolysis will more definitively address these possibilities. Regardless of the underlying mechanisms, our invasion results suggest that excessively high MRTF activity may not be optimal for ECM invasion of tumor cells.

In this study, we demonstrate DIAPH3 upregulation as a key mechanism underlying MRTF-stimulated cell migration. The exact mechanism by which MRTF regulates DIAPH3 expression in an SRF-dependent manner is still unclear. Although our RNAseq data shows evidence for MRTF-induced increase in DIAPH3 mRNA content in an SRF-dependent manner, as per the ENCODE project data, DIAPH1 but not DIAPH3 is a bona-fide transcriptional target of SRF (Consortium, 2004). Therefore, it is unlikely that DIAPH3 is transcriptionally regulated directly through its promoter recognition by the MRTF/SRF complex. A previous study found that mRNA-binding protein IGF2BP sustains the expression of select SRF-target genes (including SRF itself) by impairing miRNA-mediated decay of mRNA, a process that involves N^6-methyladenosine (m^6A)-modification of transcripts recognized by IGF2BP (Muller et al., 2019). Interestingly, there is also evidence for IGF2BP3-mediated increase of DIAPH3 mRNA stability involving m6A-modification of the transcripts (Wu et al., 2022). Therefore, it will be interesting to explore in the future whether MRTF-A-dependent changes in DIAPH3 expression involves IGF2BP-mediated mRNA stability control.

A number of cancer-related studies have previously documented a role of DIAPH3 in modulating tumor cell aggressiveness albeit in a context- and study-specific manner. For example, pan-cancer analyses revealed that DIAPH3 is upregulated in multiple types of human cancer (breast, cervical, head and neck squamous carcinoma, glioblastoma and several others) and serves as a prognostic manner in certain cancers(Chen et al., 2023). DIAPH3 expression is upregulated in osteosarcoma, and silencing DIAPH3 expression suppresses proliferation, migration/invasion and metastasis of osteosarcoma cells(Zhang et al., 2021). In the context of hepatocellular carcinoma (HCC), while one study documented DIPAH3's ability to stimulate migration/invasion and metastatic capability of HCC cells (Dong et al., 2018), another study found non-coding RNA-mediated exon skipping and reduced expression of DIAPH3, further linking to epithelial-mesenchymal transition, migration, invasion and metastasis of HCC cells (Su et al., 2023). Conflicting results have also been reported in the literature with regard to DIAPH3's role in breast cancer. In one study, silencing DIAPH3 induced ameboid migration promoting invasion and metastasis of oncogenic HRAS-transformed human mammary epithelial cells (Hager et al., 2012). Depletion of DIAPH3 also induces nuclear shape instability promoting migratory ability of breast and prostate cancer cells (Reis-Sobreiro et al., 2018). Contrasting these findings, another study found that all diaphanous proteins including DIAPH3 are required for invadopodia formation and efficient ECM invasion of MDA-231 breast cancer cells (Lizarraga et al., 2009). Our findings that DIAPH3 silencing reduces actin polymerization at the lamellipodial edge and reduces migration of MDA-231 cells are consistent with previously demonstrated DIAPH3's role in lamellipodial protrusion (Yang et al., 2007). Although we are able to reconcile our findings with anti-migratory effect of DIAPH3 in breast cancer cells as shown in some of the previous studies (Hager et al., 2012, Reis-Sobreiro et al., 2018), we speculate study-specific differences in model systems and experimental assays may partly underlie the dichotomy in the findings.

Only a handful of studies to date have assessed MRTF expression/activity in human BC. One study found higher mRNA expression of MRTF-A and a select MRTF-A target genes (ACTA2/α-smooth-muscle actin, SM22/TAGLN, CD49e/integrin-α5, and CCN2/CTGF) in the primary tumor associated with shorter overall survival of a small set of luminal (n=129) and mixed (n=104) breast cancer patient cohorts (Seifert and Posern, 2017). Another study revealed MRTF-A's SRF-independent/SAP-dependent gene expression as a prognostic signature of highly proliferative BC with adverse clinical outcome (Gurbuz et al., 2014).

However, these studies involved gene expression analyses of bulk tumor, which does not distinguish the effect of MRTF in tumor cell from stromal cell populations. We also recognize that the overall survival data is influenced by various aspects of tumor cell behavior (growth, dissemination, and survival) in addition to other patient-specific confounding variables that are unrelated to cancer. Therefore, we currently lack an explicit understanding of whether tumor-cell-intrinsic expression/sub-cellular localization of any particular isoform of MRTF is correlated specifically with malignancy-associated features in human BC. Our TMA IHC data showed that cancer cells infiltrated in the stromal region have higher N/C ratio of both MRTF-A and MRTF-B relative to those present in the bulk tumor. A possible interpretation of this finding could be that invading subpopulation of tumor cells upregulate MRTF activity. Interestingly, N/C ratio of only MRTF-A (but not MRTF-B) in cancer cells exhibited a positive correlation with lymph node infiltration in TNBC. The underlying reasons for isoform-specific selectivity of MRTF for association with lymph node infiltration in TNBC are not clear. However, since lymph node infiltration also involves intravasation, there might be isoform-specific effect of MRTF activity in cancer cells on endothelial barrier disruption (a key aspect of intravasation) which will need to be investigated in the future. Encouragingly, we provide clinical evidence for elevated SRF-specific gene signature of MRTF in distant metastases relative to matched primary tumor in human disease, a finding that is consistent with critical importance of MRTF/SRF transcriptional axis for tumor cell migration and invasion. However, since MRTF/SRF activity is also critical for tumor initiation and metastatic outgrowth of breast cancer cells (Gau et al., 2022), MRTF-dependence for metastatic outgrowth could an additional contributory reason for elevated MRTF/SRF activity in distant metastases.

EXPERIMENTAL PROCEDURES

*Cell culture and transfection***.** Generation and culture of GFP/luciferase-expressing sublines of MDA-231 expressing various dox-inducible MRTF-A constructs have been recently reported by our group(Gau et al., 2022). D2A1 cell line (originally provided to us by Dr. William Schiemann, Case Western Reserve University) were transduced with lentivirus encoding either MRTF-A/B shRNA (Vectorbuilder vector ID - VB200825-1246dwj) or non-targeting control shRNA (Vectorbuilder vector ID - VB151023-10034), and selected/maintained with puromycin in DMEM media supplemented with FBS (Corning, catalog# MT35011CV) and antibiotics (100 U/ml penicillin and 100 µg/ml streptomycin; Thermo Fisher, catalog# 15070063. For transient gene silencing, siRNAs were transfected using Lipofectamine RNAiMAX (Thermo Fisher, catalog #13778100). The following siRNA were used at a concentration of 2.5nM (MRTF-A and -B) or 5nM (DIAPH3): custom single target 3' UTR MRTF-A (Dharmacon – Sequence: 5'-GUGUCUUGGUGUAGUGUAAUU-3'), Smart-Pool MRTF-B siRNA (Santa Cruz, catalog #sc-61074), and Smart-Pool DIAPH3 siRNA (Dharmacon Catalog ID: E-018997-00-0005).

*Immunoblotting***.** Total lysate was extracted in Pierce™ IP Lysis buffer (Thermo Scientific – Catalog #87787) containing 0.3% SDS. Prior to loading samples in the acrylamide gel the samples were boiled in 1X sample buffer. For immunoblotting, the following antibodies at the following concentrations were used: Polyclonal anti-MRTF-A antibody (Abcam-ab113264; 1:1000), Polyclonal anti-MRTF-B antibody (abcam – ab235101; 1:1000), polyclonal anti-GAPDH antibody (Sigma Aldrich – ABS16; 1:1000), monoclonal anti-mCherry antibody (Cell Signaling – E5D8F; 1:1000), polyclonal anti-DIAPH3 (Abcam – ab245660; 1:1000), and polyclonal DIAPH1 antibody (Abcam – ab11173; 1:1000).

*Time-lapse cell motility assay***.** Cells were sparsely plated on collagen coated (10µg/ml) 24-well plate overnight and imaged for 3h at 10 min intervals with a 10x objective. The onstage environmental chamber was maintained at 37°C and 5% CO_2 for the entire duration of time-lapse imaging. Multiple beacons for imaging were selected for frames with single cells in each well. Cells were segmented and tracked using Ilastik(Berg et al., 2019) and trajectories were constructed using centroid coordinates of cell areas. Only

cells that were present in the imaging frame for greater than 2 hours were counted. Persistence, shown as standard deviation of $\Delta\theta$, was calculated using $\Delta\theta$ with $\theta_{i,\,i+1} = \cos^{-1}(x_{i+1} - x_i)/\text{sqrt}\,((x_{i+1} - x_i)^2) + ((y_{i+1} - y_i)^2)$ where x and y are the position coordinates. For experiments involving dox-inducible overexpression, cells were treated with dox for 48h prior to imaging. For experiments involving gene knockdown, time-lapse imaging studies were performed 72h after siRNA transfection.

*Spheroid invasion assay***.** Spheroids composed of 3000 uninduced (i.e., non-doxycycline treated) cells were formed for 48 hours in 10µg/ml Collagen-1 (Gibco - Catalog #A10483-01) in the wells of a round-bottom, low-adhesion 96-well plates (Corning – product number 7007). After 48 hours of formation, 1µg/ml doxycycline was added to the wells for 24 hours. Collagen-1 (prepared at 2 mg/ml) was added to the media in the wells to a final concentration of 1mg/ml and allowed to polymerize for 1 hour prior to the addition of serum-containing media supplemented with 1µg/ml dox. After allowing cells to invade for 96 hours, the spheroids were fixed in 3.7% formaldehyde for 1h, permeabilized overnight in 0.5% Triton-X at 4°C, and stained with DAPI and Acta-Stain 670 phalloidin (Cytoskeleton – catalog # PHDN1) overnight at 4°C. Spheroids were imaged at 0h and 96h with a 2.5X objective. However, the spheroids which were not able to be imaged (primarily due to not being in the center of the round bottom plate) were excluded from the study.

*Kymography analysis***.** Time-lapse imaging of randomly migrating cells was performed over 10 minutes at a 2-second time interval with a 20X objective. Kymographs were constructed using compiled slices of the time-lapse frames along multiple 1-pixel lines drawn across the protruding edge of a cell using ImageJ. Kymographs were then processed in ImageJ by background subtraction followed by automated local thresholding about the mean intensity. Protrusions were identified from the binary thresholded images using R. Local maxima and minima were identified in the kymographs using the following method. First, local regression (LOESS) was performed to generate a smoothed curve (plotted as a black line in **Fig 5A**) using the coordinates of the thresholded leading edge. Next, on a rolling basis the highest point in the span of 7 time points (12s) was assigned to each point along the curve. This generated a curve, herein referred to as the highest local point loess regression curve (plotted in green in **Fig 5A**). Finally, the loess regression curve was subtracted from the highest point loess regression curve. The points at which the results of the subtracted curves were equal to zero were treated as the local maxima. The same algorithm was used to identify local minima. Local maxima less than 2 pixels high were excluded from the analysis. The frequency of protrusion, net protrusion distance and duration of protrusion ascent were then calculated based on these identified local minima and maxima. For each cell, at least 2 kymographs were constructed for analysis.

*F-Actin staining***.** Cells cultured on the wells of a collagen-1-coated (10µg/ml) 24-well plates were washed with PBS, fixed with 3.7% formaldehyde for 15 minutes, permeabilized with 0.5% Triton-X for 5 minutes, and stained with Acta-Stain 670 phalloidin for 30 minutes (Cytoskeleton – catalog # PHDN1) at room temperature. Counterstaining for nuclei with DAPI was subsequently performed for 1 minute at room temperature. Fluorescence images acquired with a 20X objective were processed in ImageJ for background subtraction and automatic thersholding before quantifying the integrated intensity on a per cell basis by utilizing the "Analyze Particles" function. For wound-healing assay, cells were seeded in the wells a 24-well plate at 80% confluency and allowed to reach confluency overnight. A wound was made in each well using a 200 µl pipet tip, and cells were allowed to migrate for 3 hours before performing phalloidin staining and fluorescence image acquisition of the leading edge as described above. Images thresholded for phalloidin-positive region were exported to R for calculation of the average fluorescence intensity at the 2 pixels across the entire leading edge.

Multiplexed quantitative IHC. Breast cancer TMA was purchased from Yale University (YTMA 49-13) and has been used in many previous studies for cancer biomarker identification and validation (Zerkowski

et al., 2007, Giltnane et al., 2009, Chakraborty et al., 2018). The TMA was composed of spots from 647 breast cancer patient samples. After quality assessment post-staining, 360 of the spots were deemed quality and used for further evaluation. 18.6% of the samples were stage 1, 37.5% of the samples were stage 2, 26.9% of the samples were stage 3, 6.1% of the samples were stage 4, and 10.8% of the samples did not have a determined stage. 47 % of samples were ER+ and 53% of samples were ER- as determined by the histology score (a score of 0 or 1 was counted as ER-). This TMA was specifically procured to have approximately equal numbers of ER- and ER+ samples. Automated staining of TMA was performed on the Leica Bond RX. For staining, Akoya Bioscience's Opal 6-Plex Detection Kit (cat# NEL871001KT) was used according to the manufacturer's instructions. The antibodies used in the staining process are as follows: MRTF-A (abcam – ab43269 – 1:200), MRTF-B (abcam – ab235101 – 1:500), and pan-cytokeratin (Clone AE1/AE3 – Santa Cruz – sc81714 – 1:150). Akoya Bioscience's PhenoimagerHT platform was used for whole slide scanning. Akoya Biosciences InForm® analysis software was used for spectral unmixing, tissue/cell segmentation, and phenotyping. The minimum size threshold to be counted as a tumor region was 2000 pixels. Any single or clusters of pan-CK+ cells less than 2000 pixels were counted as cancer cells present in the stroma compartment.

RNA-sequencing and gene signature construction. For RNA sequencing, MDA-231 cells were cultured on either 2D tissue culture dishes or on top of 3D matrigel substrate (as per protocol of matrigel-on-top culture detailed in(Gau et al., 2022), and induced with dox for 72h for transgene (WT vs mutant forms of MRTF-A) expression prior to RNA-collection with the Qiagen RNeasy Mini Plus Kit following manufacturer's protocol. Samples were submitted to the University of Pittsburgh HSCRF Genomics Research Core for RNA-sequencing. The core facility prepared the RNA library using TruSeq Stranded Total Ligation (Ribo-Zero Plus) protocol (Illumina) and performed paired-end reads on the Illumina NextSeq 2000 platform. Samples were sequenced to a minimum of 22 million reads per sample. Quality of sequencing reads was determined with FastQC before transcripts from the Ensembl v.93 transcriptome (hg38) were quantified with Salmon v0.14.0. Gene-level expression was calculated using tximport v.1.12.0, differential gene expression was calculated with DESeq2 v.1.24.0, and BiomaRt v.2.46.0 was used to annotate gene names. Genes with a minimum expression value greater than 1 transcripts per million (TPM) in either control or experimental group, an adjusted *p*-value less than 0.01, and an absolute Log_2fold change greater than 1.5 were considered differentially expressed. Raw read data and processed data can be accessed from an SRA/GEO submission that is currently in progress. Procedures of gene signature generation are detailed in the "Results" section. GSVA package was used to calculate the ssGSEA scores (Hanzelmann et al., 2013).

Transcriptome analyses of paired primary and metastatic breast tumors. The dataset consists of 51 pairs of primary and paired metastases from cohort in University of Pittsburgh. DNA/RNA was extracted from formalin-fixed paraffin-embedded (FFPE) tissue from patient-matched primary breast tumors and resected metastases using the Qiagen GeneRead DNA FFPE kit using standard protocols. Sample quality and concentration were assessed by Qubit and fragment analysis. RNA library was prepared with TruSeq Stranded Total RNA (Degraded RNA) v2 RNA Exome Library and TS RNA Access capture protocol (Illumina), and RNA expression passing quality control was quantified with Salmon and normalized in log-normalized counts before ssGSEA calculation. Detailed description of data processing is as described in (Cosgrove et al., 2022).

*Statistics and data representation***.** All statistical tests were performed in GraphPad Prism 9 software. Specifics of statistical tests are indicated in the figure legends. Data were plotted in GraphPad Prism 9 or in R (ggplot2).

ACKNOWLDEGMENTS

IE was supported by NIBIB T32-EB001026 and NCATS TL1-TR001858 pre-doctoral training grants. VY was supported by a summer research internship from the School of Engineering at University of Pittsburgh. DG was supported by a National Cancer Center fellowship, NCI K99-CA267180 and T32-HL129964. Work in the Roy lab was supported by grants from NIH (R01CA248873, R01CA271095, and R21EY032632). Fangyuan Chen was a former visiting research scholar at the University of Pittsburgh School of Medicine supported by funds from The China Scholarship Council and Tsinghua University.

AUTHOR CONTRIBUTIONS

IE designed experiments, performed experiments, analyzed data, and wrote manuscript; VY and DG performed experiments and analyzed data, MJ performed experiments, analyzed data and wrote manuscript, DB and FC performed data analyses and wrote manuscript; AVL and PL oversaw some aspects of data analyses, PR conceived the overall study design, supervised the project, oversaw experiments, edited/wrote manuscript and acquired funding.

CONFLICT OF INTEREST: The authors declare no competing conflict of interest.

REFERNCES

ASPARUHOVA, M. B., SECONDINI, C., RUEGG, C. & CHIQUET-EHRISMANN, R. 2015. Mechanism of irradiation-induced mammary cancer metastasis: A role for SAP-dependent MkI1 signaling. *Mol Oncol,* 9**,** 1510-27.

BERG, S., KUTRA, D., KROEGER, T., STRAEHLE, C. N., KAUSLER, B. X., HAUBOLD, C., SCHIEGG, M., ALES, J., BEIER, T., RUDY, M., EREN, K., CERVANTES, J. I., XU, B., BEUTTENMUELLER, F., WOLNY, A., ZHANG, C., KOETHE, U., HAMPRECHT, F. A. & KRESHUK, A. 2019. ilastik: interactive machine learning for (bio)image analysis. *Nat Methods,* 16**,** 1226-1232.

CHAKRABORTY, S., JIANG, C., GAU, D., ODDO, M., DING, Z., VOLLMER, L., JOY, M., SCHIEMANN, W., STOLZ, D. B., VOGT, A., GHOSH, S. & ROY, P. 2018. Profilin-1 deficiency leads to SMAD3 upregulation and impaired 3D outgrowth of breast cancer cells. *Br J Cancer,* 119**,** 1106-1117.

CHEN, X., XIE, L., QIAO, K., ZHU, X., REN, J. & TAN, Y. 2023. The pan-cancer analysis identified DIAPH3 as a diagnostic biomarker of clinical cancer. *Aging (Albany NY),* 15**,** 689-704.

CONSORTIUM, E. P. 2004. The ENCODE (ENCyclopedia Of DNA Elements) Project. *Science,* 306**,** 636-40.

COSGROVE, N., VARESLIJA, D., KEELAN, S., ELANGOVAN, A., ATKINSON, J. M., COCCHIGLIA, S., BANE, F. T., SINGH, V., FURNEY, S., HU, C., CARTER, J. M., HART, S. N., YADAV, S., GOETZ, M. P., HILL, A. D. K., OESTERREICH, S., LEE, A. V., COUCH, F. J. & YOUNG, L. S. 2022. Mapping molecular subtype specific alterations in breast cancer brain metastases identifies clinically relevant vulnerabilities. *Nat Commun,* 13**,** 514.

COSTELLO, P., SARGENT, M., MAURICE, D., ESNAULT, C., FOSTER, K., ANJOS-AFONSO, F. & TREISMAN, R. 2015. MRTF-SRF signaling is required for seeding of HSC/Ps in bone marrow during development. *Blood,* 125**,** 1244-55.

DONG, L., LI, Z., XUE, L., LI, G., ZHANG, C., CAI, Z., LI, H. & GUO, R. 2018. DIAPH3 promoted the growth, migration and metastasis of hepatocellular carcinoma cells by activating beta-catenin/TCF signaling. *Mol Cell Biochem,* 438**,** 183-190.

EVELYN, C. R., BELL, J. L., RYU, J. G., WADE, S. M., KOCAB, A., HARZDORF, N. L., SHOWALTER, H. D., NEUBIG, R. R. & LARSEN, S. D. 2010. Design, synthesis and prostate cancer cell-based studies of analogs of the Rho/MKL1 transcriptional pathway inhibitor, CCG-1423. *Bioorg Med Chem Lett,* 20**,** 665-72.

FRANCO, C. A., BLANC, J., PARLAKIAN, A., BLANCO, R., ASPALTER, I. M., KAZAKOVA, N., DIGUET, N., MYLONAS, E., GAO-LI, J., VAAHTOKARI, A., PENARD-LACRONIQUE, V., FRUTTIGER, M., ROSEWELL, I., MERICSKAY, M., GERHARDT, H. & LI, Z. 2013. SRF selectively controls tip cell invasive behavior in angiogenesis. *Development,* 140**,** 2321-33.

GAU, D., CHAWLA, P., EDER, I. & ROY, P. 2022. Myocardin-related transcription factor's interaction with serum-response factor is critical for outgrowth initiation, progression, and metastatic colonization of breast cancer cells. *FASEB Bioadv,* 4**,** 509-523.

GAU, D. & ROY, P. 2018. SRF'ing and SAP'ing - the role of MRTF proteins in cell migration. *J Cell Sci,* 131.

GAU, D., VEON, W., CAPASSO, T. L., BOTTCHER, R., SHROFF, S., ROMAN, B. L. & ROY, P. 2017. Pharmacological intervention of MKL/SRF signaling by CCG-1423 impedes endothelial cell migration and angiogenesis. *Angiogenesis,* 20**,** 663-672.

GIESE, A., BJERKVIG, R., BERENS, M. E. & WESTPHAL, M. 2003. Cost of migration: invasion of malignant gliomas and implications for treatment. *J Clin Oncol,* 21**,** 1624-36.

GIESE, A., KLUWE, L., LAUBE, B., MEISSNER, H., BERENS, M. E. & WESTPHAL, M. 1996a. Migration of human glioma cells on myelin. *Neurosurgery,* 38**,** 755-64.

GIESE, A., LOO, M. A., TRAN, N., HASKETT, D., COONS, S. W. & BERENS, M. E. 1996b. Dichotomy of astrocytoma migration and proliferation. *Int J Cancer,* 67**,** 275-82.

GILTNANE, J. M., MOEDER, C. B., CAMP, R. L. & RIMM, D. L. 2009. Quantitative multiplexed analysis of ErbB family coexpression for primary breast cancer prognosis in a large retrospective cohort. *Cancer,* 115**,** 2400-9.

GORELIK, R., YANG, C., KAMESWARAN, V., DOMINGUEZ, R. & SVITKINA, T. 2011. Mechanisms of plasma membrane targeting of formin mDia2 through its amino terminal domains. *Mol Biol Cell,* 22**,** 189-201.

GUALDRINI, F., ESNAULT, C., HORSWELL, S., STEWART, A., MATTHEWS, N. & TREISMAN, R. 2016. SRF Co-factors Control the Balance between Cell Proliferation and Contractility. *Mol Cell,* 64**,** 1048-1061.

GURBUZ, I., FERRALLI, J., ROLOFF, T., CHIQUET-EHRISMANN, R. & ASPARUHOVA, M. B. 2014. SAP domain-dependent Mkl1 signaling stimulates proliferation and cell migration by induction of a distinct gene set indicative of poor prognosis in breast cancer patients. *Mol Cancer,* 13**,** 22.

HAGER, M. H., MORLEY, S., BIELENBERG, D. R., GAO, S., MORELLO, M., HOLCOMB, I. N., LIU, W., MOUNEIMNE, G., DEMICHELIS, F., KIM, J., SOLOMON, K. R., ADAM, R. M., ISAACS, W. B., HIGGS, H. N., VESSELLA, R. L., DI VIZIO, D. & FREEMAN, M. R. 2012. DIAPH3 governs the cellular transition to the amoeboid tumour phenotype. *EMBO Mol Med,* 4**,** 743-60.

HAN, Z., LI, X., WU, J. & OLSON, E. N. 2004. A myocardin-related transcription factor regulates activity of serum response factor in Drosophila. *Proc Natl Acad Sci U S A,* 101**,** 12567-72.

HANZELMANN, S., CASTELO, R. & GUINNEY, J. 2013. GSVA: gene set variation analysis for microarray and RNA-seq data. *BMC Bioinformatics,* 14**,** 7.

HAYASHI, K., WATANABE, B., NAKAGAWA, Y., MINAMI, S. & MORITA, T. 2014. RPEL proteins are the molecular targets for CCG-1423, an inhibitor of Rho signaling. *PLoS One,* 9**,** e89016.

HOLSTEIN, I., SINGH, A. K., POHL, F., MISIAK, D., BRAUN, J., LEITNER, L., HUTTELMAIER, S. & POSERN, G. 2020. Post-transcriptional regulation of MRTF-A by miRNAs during myogenic differentiation of myoblasts. *Nucleic Acids Res,* 48**,** 8927-8942.

LIZARRAGA, F., POINCLOUX, R., ROMAO, M., MONTAGNAC, G., LE DEZ, G., BONNE, I., RIGAILL, G., RAPOSO, G. & CHAVRIER, P. 2009. Diaphanous-related formins are required for invadopodia formation and invasion of breast tumor cells. *Cancer Res,* 69**,** 2792-800.

MEDJKANE, S., PEREZ-SANCHEZ, C., GAGGIOLI, C., SAHAI, E. & TREISMAN, R. 2009. Myocardin-related transcription factors and SRF are required for cytoskeletal dynamics and experimental metastasis. *Nature Cell Biology,* 11**,** 257-U85.

MIRALLES, F., POSERN, G., ZAROMYTIDOU, A. I. & TREISMAN, R. 2003. Actin dynamics control SRF activity by regulation of its coactivator MAL. *Cell,* 113**,** 329-42.

MOUILLERON, S., LANGER, C. A., GUETTLER, S., MCDONALD, N. Q. & TREISMAN, R. 2011. Structure of a pentavalent G-actin*MRTF-A complex reveals how G-actin controls nucleocytoplasmic shuttling of a transcriptional coactivator. *Sci Signal,* 4**,** ra40.

MULLER, S., GLASS, M., SINGH, A. K., HAASE, J., BLEY, N., FUCHS, T., LEDERER, M., DAHL, A., HUANG, H., CHEN, J., POSERN, G. & HUTTELMAIER, S. 2019. IGF2BP1 promotes SRF-dependent transcription in cancer in a m6A- and miRNA-dependent manner. *Nucleic Acids Res,* 47**,** 375-390.

NAKAMURA, S., HAYASHI, K., IWASAKI, K., FUJIOKA, T., EGUSA, H., YATANI, H. & SOBUE, K. 2010. Nuclear import mechanism for myocardin family members and their correlation with vascular smooth muscle cell phenotype. *J Biol Chem,* 285**,** 37314-23.

PANAYIOTOU, R., MIRALLES, F., PAWLOWSKI, R., DIRING, J., FLYNN, H. R., SKEHEL, M. & TREISMAN, R. 2016. Phosphorylation acts positively and negatively to regulate MRTF-A subcellular localisation and activity. *Elife,* 5.

PAWLOWSKI, R., RAJAKYLA, E. K., VARTIAINEN, M. K. & TREISMAN, R. 2010. An actin-regulated importin alpha/beta-dependent extended bipartite NLS directs nuclear import of MRTF-A. *EMBO J,* 29**,** 3448-58.

POSERN, G., MIRALLES, F., GUETTLER, S. & TREISMAN, R. 2004. Mutant actins that stabilise F-actin use distinct mechanisms to activate the SRF coactivator MAL. *EMBO J,* 23**,** 3973-83.

RECORD, J., MALINOVA, D., ZENNER, H. L., PLAGNOL, V., NOWAK, K., SYED, F., BOUMA, G., CURTIS, J., GILMOUR, K., CALE, C., HACKETT, S., CHARRAS, G., MOULDING, D., NEJENTSEV, S., THRASHER, A. J. & BURNS, S. O. 2015. Immunodeficiency and severe susceptibility to bacterial infection associated with a loss-of-function homozygous mutation of MKL1. *Blood,* 126**,** 1527-35.

REIS-SOBREIRO, M., CHEN, J. F., NOVITSKAYA, T., YOU, S., MORLEY, S., STEADMAN, K., GILL, N. K., ESKAROS, A., ROTINEN, M., CHU, C. Y., CHUNG, L. W. K., TANAKA, H., YANG, W., KNUDSEN, B. S., TSENG, H. R., ROWAT, A. C., POSADAS, E. M., ZIJLSTRA, A., DI VIZIO, D. & FREEMAN, M. R. 2018. Emerin Deregulation Links Nuclear Shape Instability to Metastatic Potential. *Cancer Res,* 78**,** 6086-6097.

SCHIRENBECK, A., BRETSCHNEIDER, T., ARASADA, R., SCHLEICHER, M. & FAIX, J. 2005. The Diaphanous-related formin dDia2 is required for the formation and maintenance of filopodia. *Nat Cell Biol,* 7**,** 619-25.

SCHOEN, C. J., BURMEISTER, M. & LESPERANCE, M. M. 2013. Diaphanous homolog 3 (Diap3) overexpression causes progressive hearing loss and inner hair cell defects in a transgenic mouse model of human deafness. *PLoS One,* 8**,** e56520.

SEIFERT, A. & POSERN, G. 2017. Tightly controlled MRTF-A activity regulates epithelial differentiation during formation of mammary acini. *Breast Cancer Res,* 19**,** 68.

SOMOGYI, K. & RORTH, P. 2004. Evidence for tension-based regulation of Drosophila MAL and SRF during invasive cell migration. *Dev Cell,* 7**,** 85-93.

STASTNA, J., PAN, X., WANG, H., KOLLMANNSPERGER, A., KUTSCHEIDT, S., LOHMANN, V., GROSSE, R. & FACKLER, O. T. 2012. Differing and isoform-specific roles for the formin DIAPH3 in plasma membrane blebbing and filopodia formation. *Cell Res,* 22**,** 728-45.

SU, T., ZHANG, N., WANG, T., ZENG, J., LI, W., HAN, L. & YANG, M. 2023. Super Enhancer-Regulated LncRNA LINC01089 Induces Alternative Splicing of DIAPH3 to Drive Hepatocellular Carcinoma Metastasis. *Cancer Res,* 83**,** 4080-4094.

VARTIAINEN, M. K., GUETTLER, S., LARIJANI, B. & TREISMAN, R. 2007. Nuclear actin regulates dynamic subcellular localization and activity of the SRF cofactor MAL. *Science,* 316**,** 1749-52.

WATANABE, B., MINAMI, S., ISHIDA, H., YOSHIOKA, R., NAKAGAWA, Y., MORITA, T. & HAYASHI, K. 2015. Stereospecific Inhibitory Effects of CCG-1423 on the Cellular Events Mediated by Myocardin-Related Transcription Factor A. *PLoS One,* 10**,** e0136242.

WEINL, C., RIEHLE, H., PARK, D., STRITT, C., BECK, S., HUBER, G., WOLBURG, H., OLSON, E. N., SEELIGER, M. W., ADAMS, R. H. & NORDHEIM, A. 2013. Endothelial SRF/MRTF ablation causes vascular disease phenotypes in murine retinae. *J Clin Invest,* 123**,** 2193-206.

WU, Y., CHEN, X., BAO, W., HONG, X., LI, C., LU, J., ZHANG, D. & ZHU, A. 2022. Effect of Humantenine on mRNA m6A Modification and Expression in Human Colon Cancer Cell Line HCT116. *Genes (Basel),* 13.

YANG, C., CZECH, L., GERBOTH, S., KOJIMA, S., SCITA, G. & SVITKINA, T. 2007. Novel roles of formin mDia2 in lamellipodia and filopodia formation in motile cells. *PLoS Biol,* 5**,** e317.

ZERKOWSKI, M. P., CAMP, R. L., BURTNESS, B. A., RIMM, D. L. & CHUNG, G. G. 2007. Quantitative analysis of breast cancer tissue microarrays shows high cox-2 expression is associated with poor outcome. *Cancer Invest,* 25**,** 19-26.

ZHANG, Z., DAI, F., LUO, F., WU, W., ZHANG, S., ZHOU, R., XU, J., ZHOU, Q. & SONG, L. 2021. Diaphanous related formin 3 knockdown suppresses cell proliferation and metastasis of osteosarcoma cells. *Discov Oncol,* 12**,** 20.

ZHU, L., NARLOCH, J. L., ONKAR, S., JOY, M., BROADWATER, G., LUEDKE, C., HALL, A., KIM, R., POGUE-GEILE, K., SAMMONS, S., NAYYAR, N., CHUKWUEKE, U., BRASTIANOS, P. K., ANDERS, C. K., SOLOFF, A. C., VIGNALI, D. A. A., TSENG, G. C., EMENS, L. A., LUCAS, P. C., BLACKWELL, K. L., OESTERREICH, S. & LEE, A. V. 2019. Metastatic breast cancers have reduced immune cell recruitment but harbor increased macrophages relative to their matched primary tumors. *J Immunother Cancer,* 7**,** 265.

FIGURE LEGENDS

Figure 1. Disruption of MRTF-SRF interaction inhibits 2D random motility of BC cells. A) Schematic of the various functional domains and the mutations created to generate the ΔSAP- and ΔSRF- mutants of MRTF-A. **B)** Immunoblot data demonstrating dox-induced overexpression (OX) of wild-type (WT) and the various mutant forms of MRTF-A along with mCherry (reporter) in GFP/luciferase expressing subline of MDA-231 cells (GAPDH serves as a loading control). **C-E)** Trajectories of individual MDA-231 cells of different experimental groups in 2D time-lapse motility assay performed 48 hours of dox treatment (*panel C*). Dot plots (with indicated means) in *panels D* and *E* represent the average migration speed and the standard deviation of Δθ (a measure of the change in direction), respectively, pooled from three independent experiments with each experiment involving 4 technical replicates/group. Total number of cells analyzed in each group: control - 96, WT-MRTF-A OX 66, ΔSAP-MRTF-A OX - 65, and ΔSRF-MRTF-A OX- 69). Outliers were removed using the ROUT method (Q = 1%). One-way ANOVA was performed. **** indicates p value < 0.0001, ** indicates p value < 0.01, and * indicates p value < 0.05.

Figure 2. Disruption of MRTF-SRF interaction inhibits directed collagen invasion of tumor spheroids A) Representative images of MDA-231 tumor spheroids embedded in 1mg/ml type 1 collagen matrix at 0h (phase-contrast – 2.5X) and 96h (fluorescence staining: DAPI – 2.5X, Phalloidin – 2.5X). **B)** Quantification of the final invasive area as measured by the total DAPI+ region after 96h normalized to the size of the spheroids at 0h as measured from the phase-contrast images (control: n = 24 spheroids, WT-MRTFA OX: n = 23 spheroids, ΔSAP-MRTF-A OX: n = 18 spheroids, ΔSRF-MRTF-A OX: n = 20 spheroids). Spheroid invasion data were pooled from 7 independent experiments. Outliers were removed using the ROUT method (Q = 1%). One-way ANOVA was performed. **** indicates p value < 0.0001, ** indicates p value < 0.01, and * indicates p value < 0.05. Scale bar = 900μm.

Figure 3. Effect of disrupting MRTF-SRF interaction on lamellipodial protrusion. A) Representative kymographs constructed at the leading edge of migrating cells (time-lapse imaging was performed at 20X magnification for a total 10-minute duration at a 2-second interval) of the indicated groups of cells. The top and bottom rows are representative scans from phase-contrast images and the corresponding automated quantification of the peaks in the kymographs, respectively. The black traces represent a fitted smoothed curve calculated by local regression (LOESS) method. The green lines above the black lines represent the moving maximum point of the approximate leading front of the cells (as determined by the fitted smoothed curve) for the surrounding points (+/- 6 seconds). Local maxima indicated by the pink dots were counted when the black lines intersect the green lines. Reverse operations were performed to calculate the local minima indicated by the blue dots. **B)** Quantification of the number of protrusions per minute at each leading edge measured for the indicated groups (number of leading edgeS analyzed: control - 37, WT-MRTF-A OX - 25, ΔSAP-MRTF-A-OX - 18, and ΔSRF-MRTF-A OX - 25). **C)** Quantification of the net protrusion distance (extension distance – retraction distance) per protrusion for the indicated groups (number of protrusions analyzed: control - 320, WT-MRTF-A OX – 153, ΔSAP MRTFA OX - 137, and ΔSRF MRTFA OX - 135 protrusions). **D)** Quantification of the duration of protrusion ascent per protrusion of the indicated groups (number of protrusions analyzed: Control - 327, WT-MRTF-A OX – 160, ΔSAP-MRTF-A OX -145, and ΔSRF-MRTF-A OX -135). Kymographs were pooled across multiple fields and wells in 2 independent experiments. For all quantifications, outliers were removed using the ROUT method (Q = 1%). One-way ANOVA was performed. **** indicates p value < 0.0001, *** indicates p value < 0.001, ** indicates p value< 0.01, and * indicates p value < 0.05.

Figure 4. Effect of disruption of MRTF-SRF interaction on ABP expression in 2D and 3D culture environments. A-B) Heat-plots showing MRTF-A-dependent changes in the mRNA expression

(represented as Z-scores based on the control group's standard deviation and mean) of major classes of ABPs in MDA-231 cells based on RNA-sequencing data of cells cultured on 2D tissue culture (*panel A*) and 3D matrigel-on-top (*panel B*) substrates with 3 biological replicates. **C)** Table summarizing the list of those ABP-encoding genes which differed in expression by at least 2 Z-scores from the control group, and in the opposite directions in WT- vs ΔSRF-MRTF-A overexpression group.

Figure 5. DIAPH3 is a key mediator of MRTF-A induced promotion of cell motility and actin polymerization at the leading edge. A) Immunoblot data showing the expression of DIAPH1 and DIAPH3 after 48h dox treatment in the indicated cell lines (GAPDH and tubulin blots serves as the loading controls for DIAPH3 and DIAPH1, respectively). **B-C)** Immunoblot data showing changes in DIAPH1 and DIAPH3 expression in MDA-231 *(panel B*) and D2A1 (*panel C*) cells after transient and stable knockdown of MRTF isoforms, respectively. GAPDH and tubulin blots serve as the loading controls. **D-E)** Dot blots (with indicated means) in *panel D* represent the average migration speed of control vs MRTF-A overexpressing MDA-231 cells 72 hrs after siRNA-mediated knockdown of DIAPH3 in 2D motility assays. As control, each group of cells was transfected with non-targeting control (con) siRNA. Dox-induced MRTF-A overexpression was turned on for 48 hrs before cells were subjected to siRNA transfection. Number of cells pooled from 3 independent experiments (with 4 technical replicates/group/experiment) analyzed in each group: control (si-Con) – 78, control (si-DIAPH3) – 79, WT-MRTF-A OX (si-Con) – 73, and WT-MRTF-A OX (si-DIAPH3) – 56. Immunoblot in *panel E* demonstrates DIAPH3 knockdown (tubulin blot – loading control). **F-G)** Representative phalloidin staining images (*panel F;* scale bar = 10µm) at the migrating front of a wound-healing assay and quantification of mean phalloidin intensity at the leading edge of cells (*panel G*) (images were acquired 3 hours after the monolayer was scratched, and 9 leading fronts were analyzed/group. Data points are pooled from 3 independent experiments with 3 technical replicates per experiment. For all quantification, the ROUT method (Q = 1%) was used to remove outliers. One-way ANOVA was used to compare means. **** indicates p value < 0.0001, *** indicates p value < 0.001, ** indicates p value< 0.01, and * indicates p value < 0.05. **H**) A proposed schematic model of MRTF/SRF axis-directed stimulation of cell migration utilizing DIAPH3-mediated actin polymerization at the leading edge.

Figure 6. Multiplexed quantitative IHC-based assessment of association between subcellular localization of MRTF isoforms and malignancy-associated features in human BC. A, D) Representative images of a breast cancer TMA spot showing the tumor microenvironment stained for various markers including MRTF-A, MRTF-B, pan-cytokeratin (Pan-CK), and DAPI. Scale bar = 100µm. **B, E)** Representative images of the segmentation of TMA spots into tumor and stromal regions. Tumor regions are overlayed with the grey projection. **C, F)** Zoomed-in regions of TMA from the indicated regions of panel B and E showing expression and sub-cellular localization of MRTF-A and MRTF-B isoforms in cells, respectively. Pan-CK+ cells were identified as cancer cells. The dotted white line indicates the tumor regions and the white asterisk marks Pan-CK+ cells in the stroma. Scale bar = 25µm. **G, J)** Quantification of the average MRTF-A (*panel G*) and -B (*panel J*) expression of Pan-CK+ cells in the segmented tumor and stromal regions. (p value < 0.0001, n = 339 samples). **H, K)** Quantification of the average nuclear-to-cytoplasmic (N/C) ratio of MRTF-A (*panel H*) and -B (*panel K*) in Pan-CK+ cells in the segmented tumor and stromal regions (p < 0.0001, n = 339 samples). The N/C ratio was determined by dividing the mean MRTF intensity in the nuclear area by the mean MRTF intensity in the cytoplasmic area in an isoform-specific manner. **I, L)** Correlation plots showing the association between the number of positive lymph nodes and N/C ratio of the individual MRTF isoform (*panel I*: MRTF-A; *panel L* – MRTF-B) in Pan-CK+ cells collectively from the tumor and stroma compartments in TNBC (the histology grading scores for HER2, ER, and PR of these tumor samples were determined to be either 0 or 1).

Figure 7. Evidence for elevated MRTF-SRF gene signature in distant soft tissue metastases relative to primary tumors in human BC. A) Venn Diagrams representing the overlap of DEGs between the indicated groups to identify genes that are negatively (left) and positively (right) regulated by MRTF-A (cutoffs: absolute Log_2fold change > 1.5, false-discovery rate (FDR) <0.001, and expression level cut-off =0.1 TPM). **B)** Table showing the composition of the calculated gene signature scores constructed from the overlapping Venn diagrams. Differential gene signatures capturing both positive and negative functions of MRTF-A were generated by subtracting the positive gene signature scores from the negative gene signature scores as indicated. **C-D)** Comparison of MRTF gene signature scores (GSS) in metastases *vs* pair-matched primary tumors (panel C - individual metastatic site, and panel D – all soft tissue sites (GI tract, ovary and brain) combined). A non-parametric Wilcoxon-rank sum test with false discovery rate correction was used to compare the median GSS between groups (the adjusted p-values are indicated above the plots).

Eder et al. Figure 1

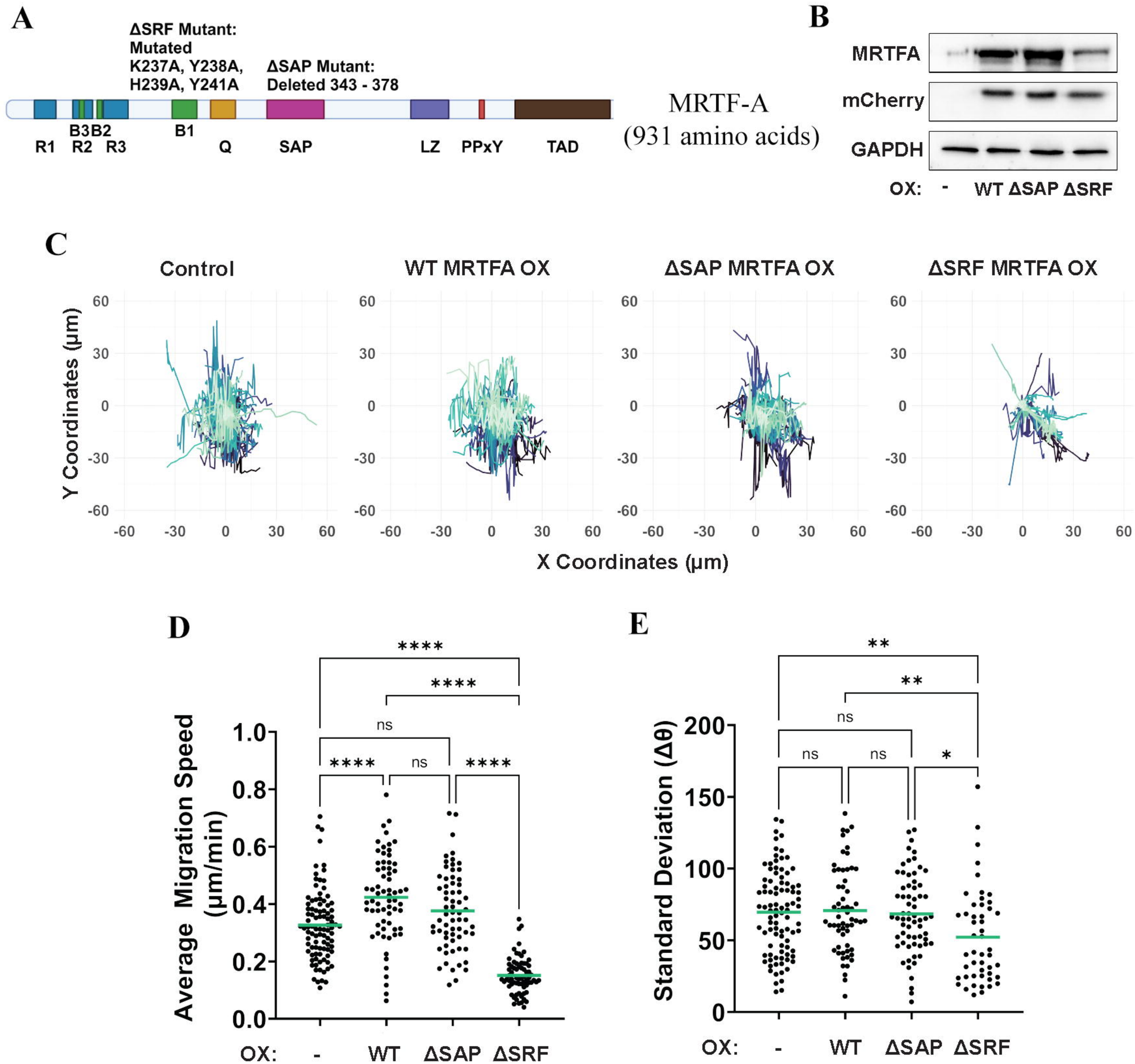

Eder et al. Figure 2

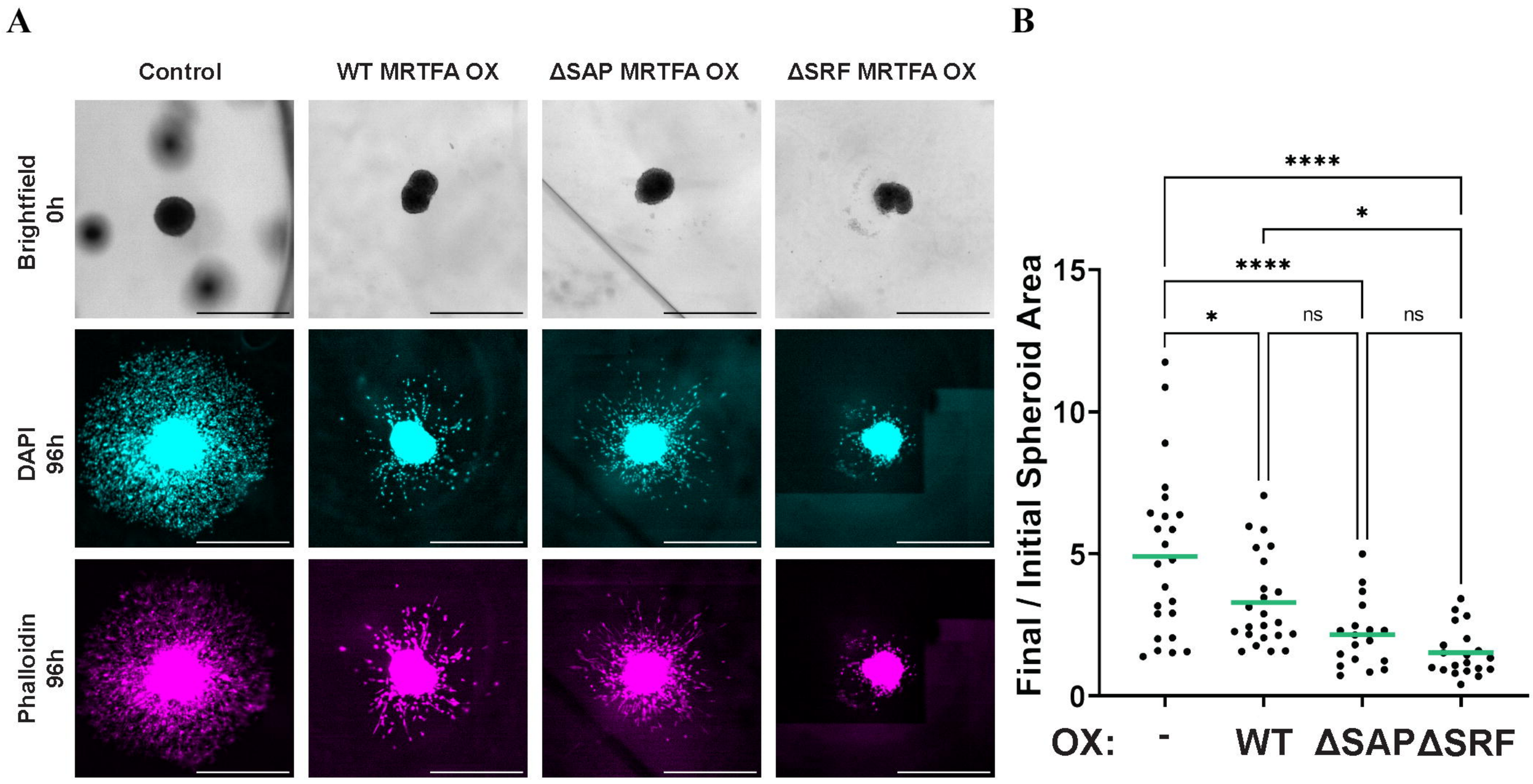

Eder et al. Figure 3

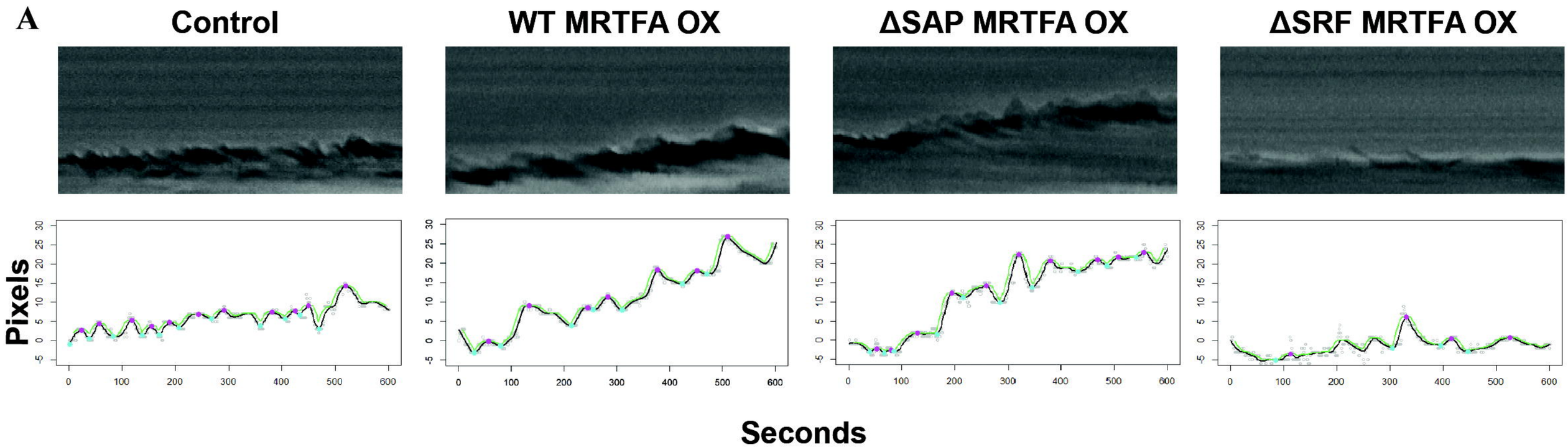

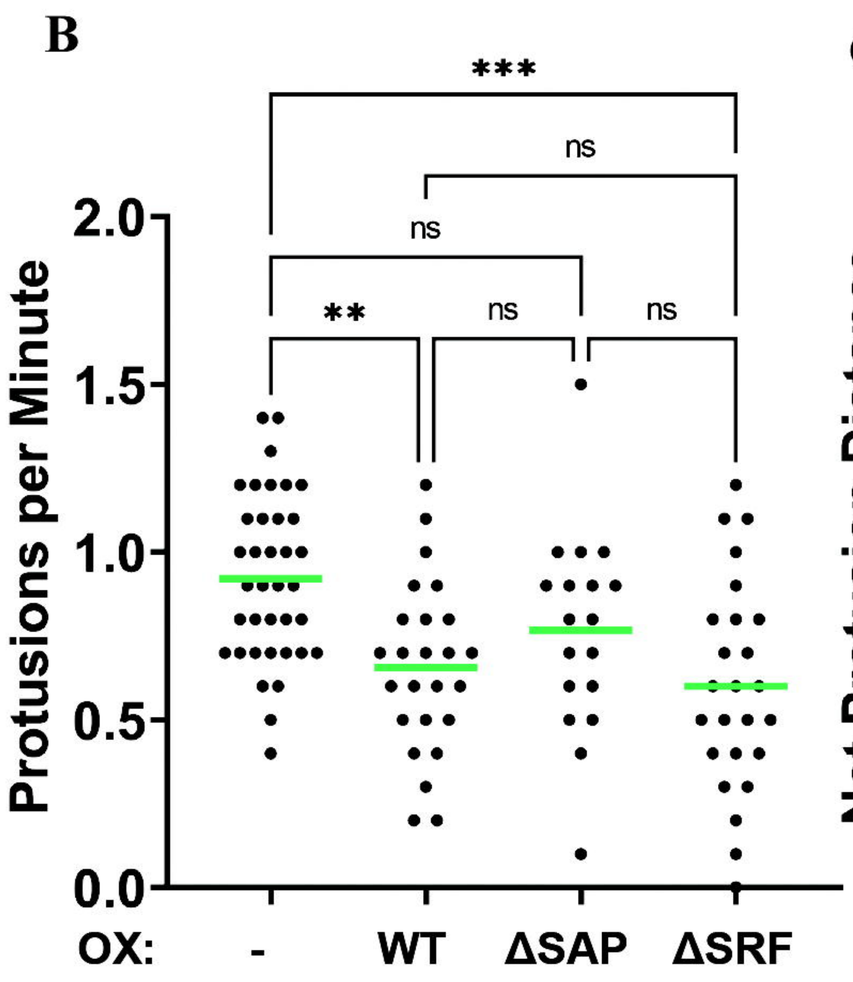

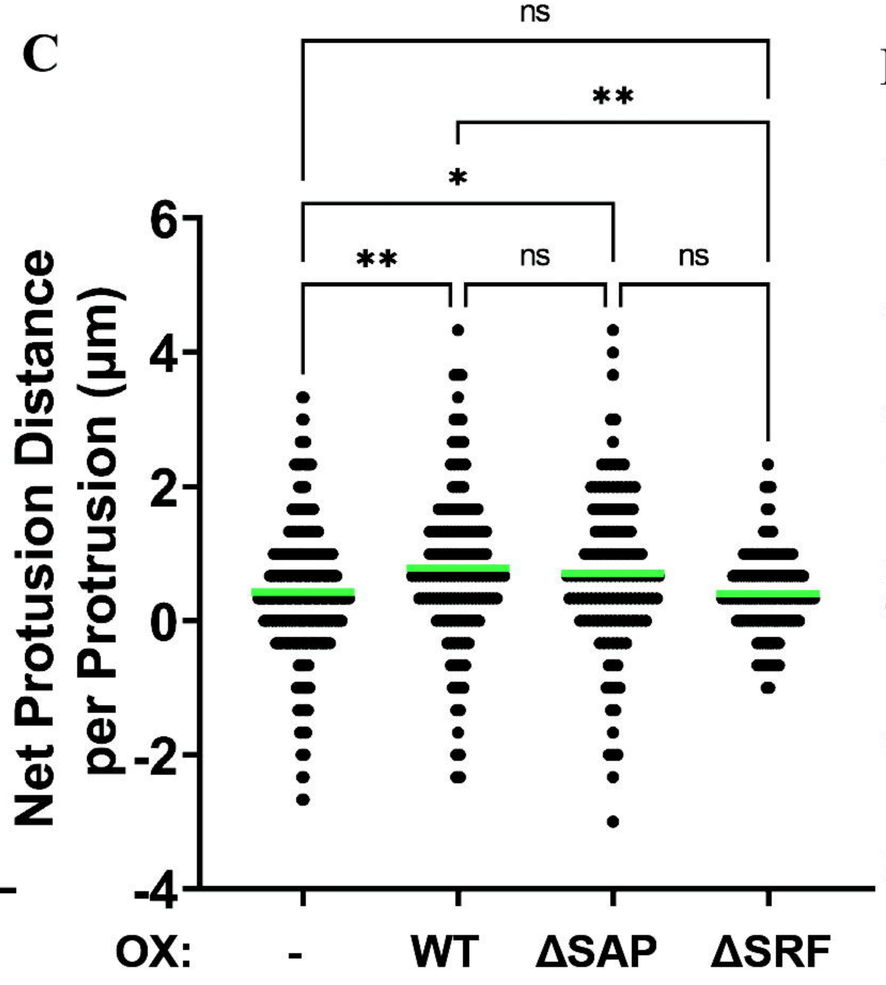

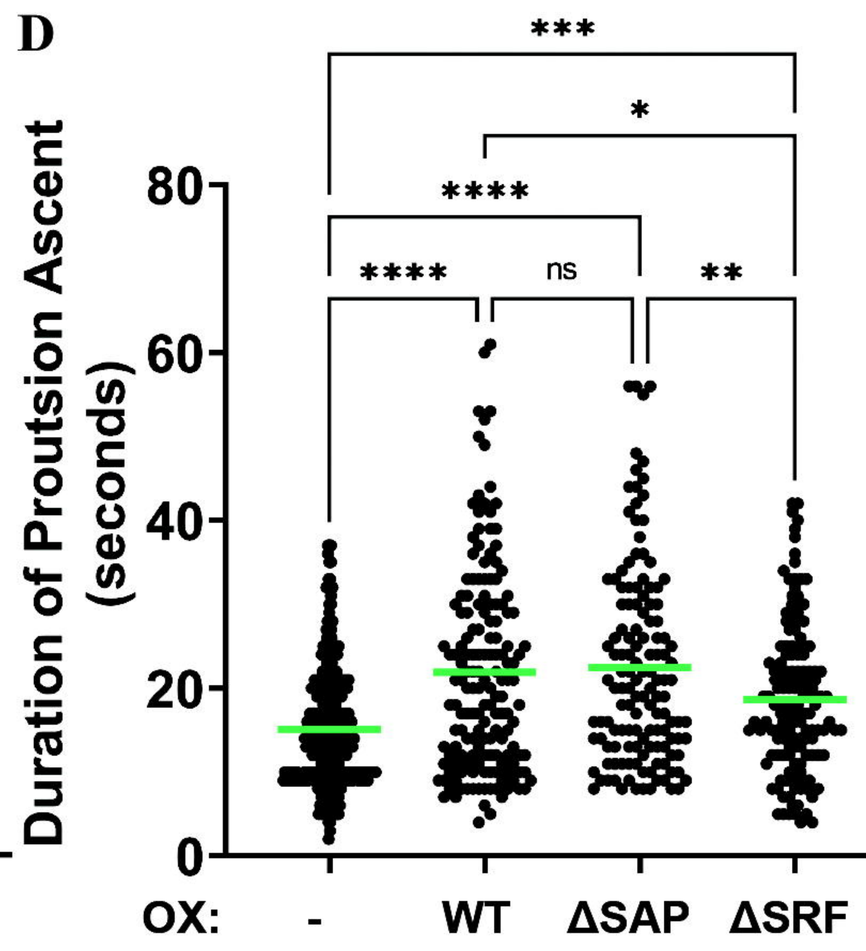

Eder et al. Fig 4

A

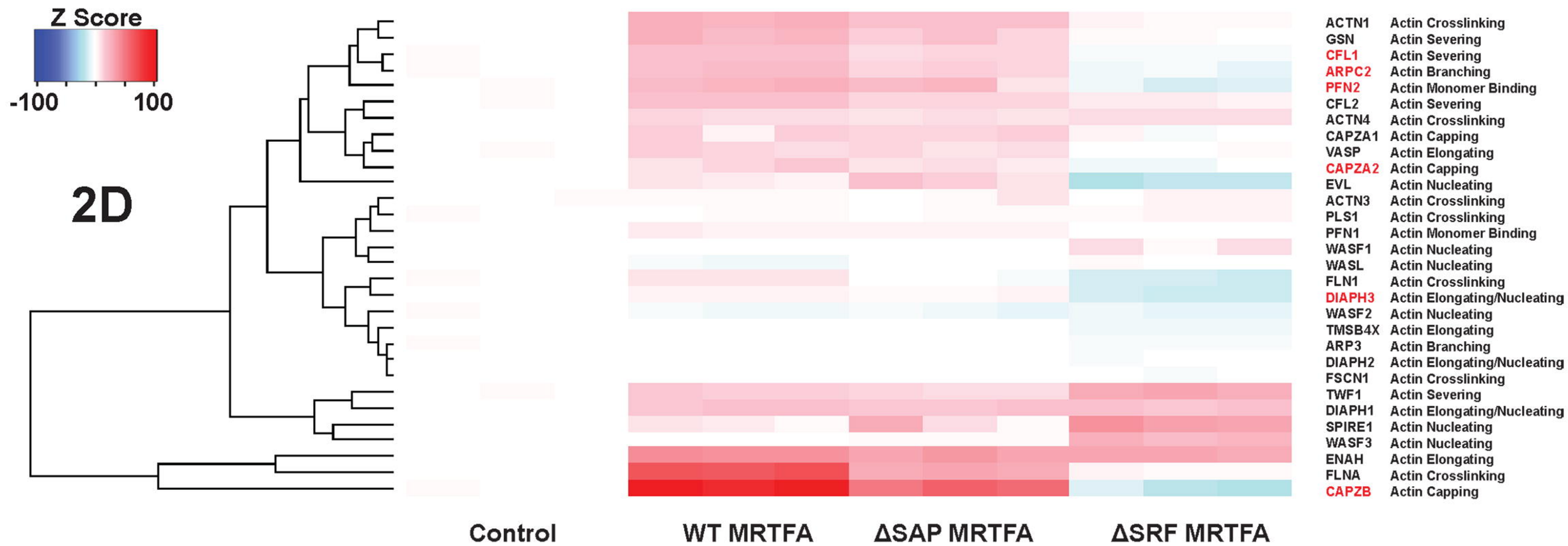

B

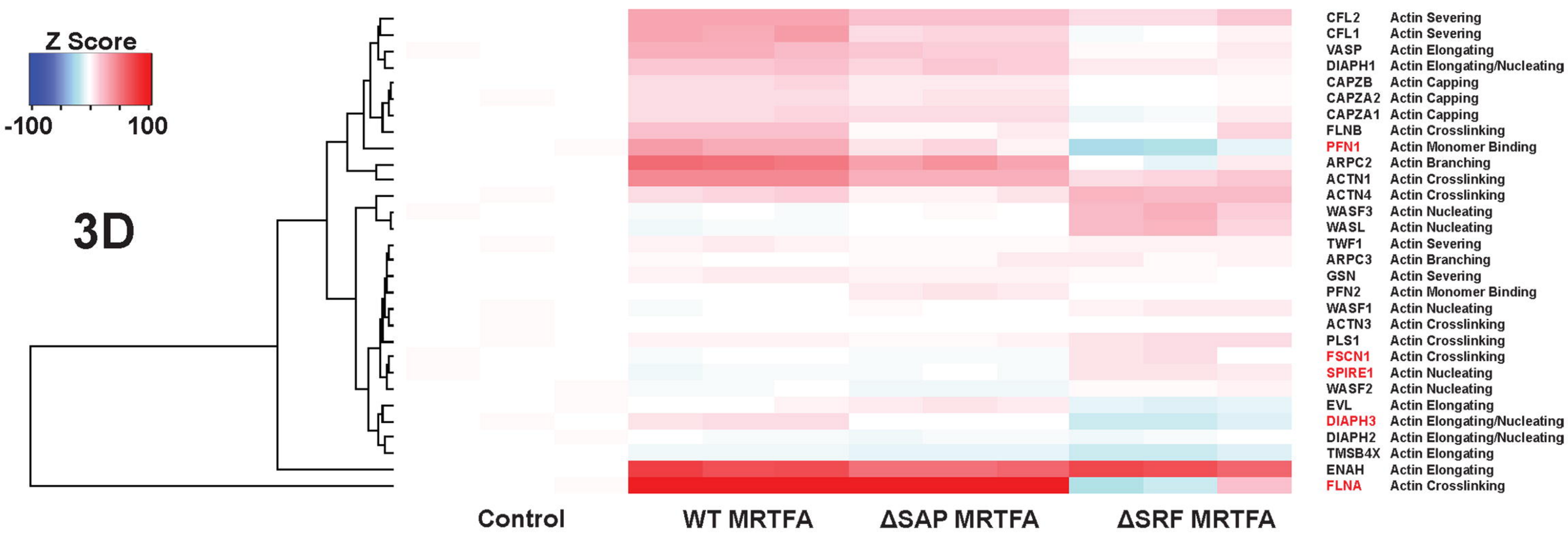

C

	2D	3D
CFL1	X	
ARPC2	X	
PFN2	X	
CAPZA2	X	
DIAPH3	X	X
CAPZB	X	
PFN1		X
FSCN1		X
SPIRE1		X
FLNA		X

Eder et al. Fig 5

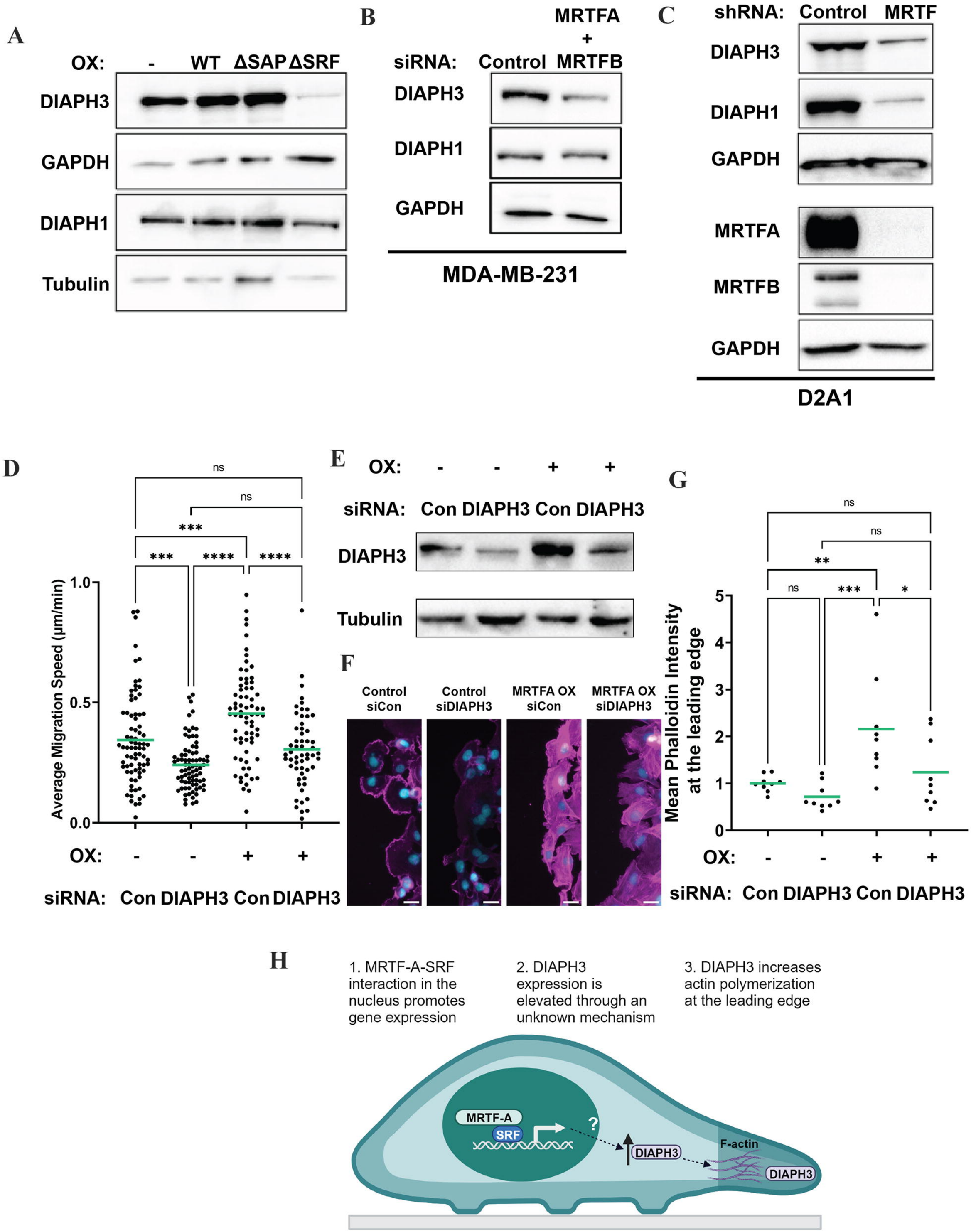

Eder et al. Figure 6

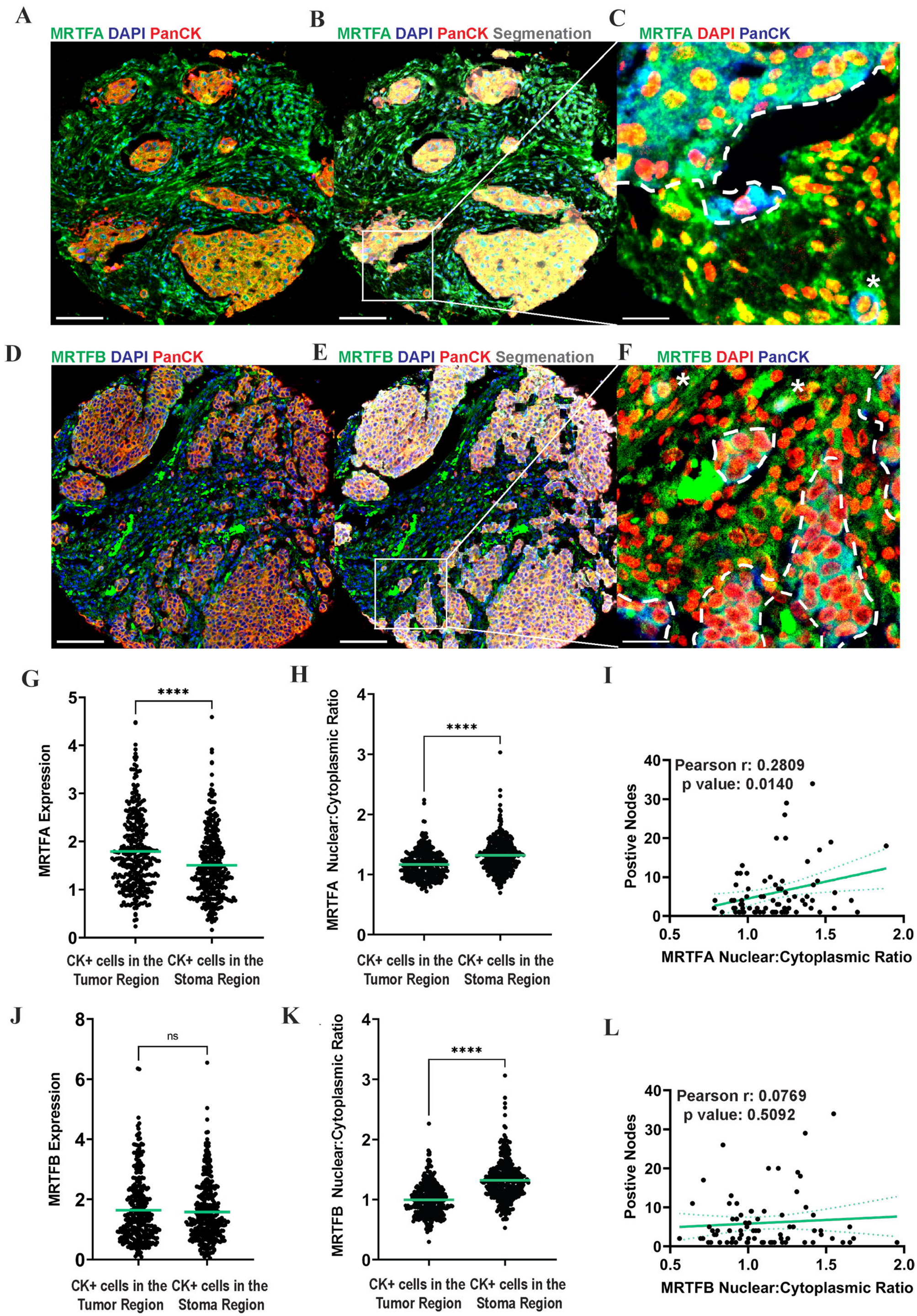

Eder et al. Fig 7

A

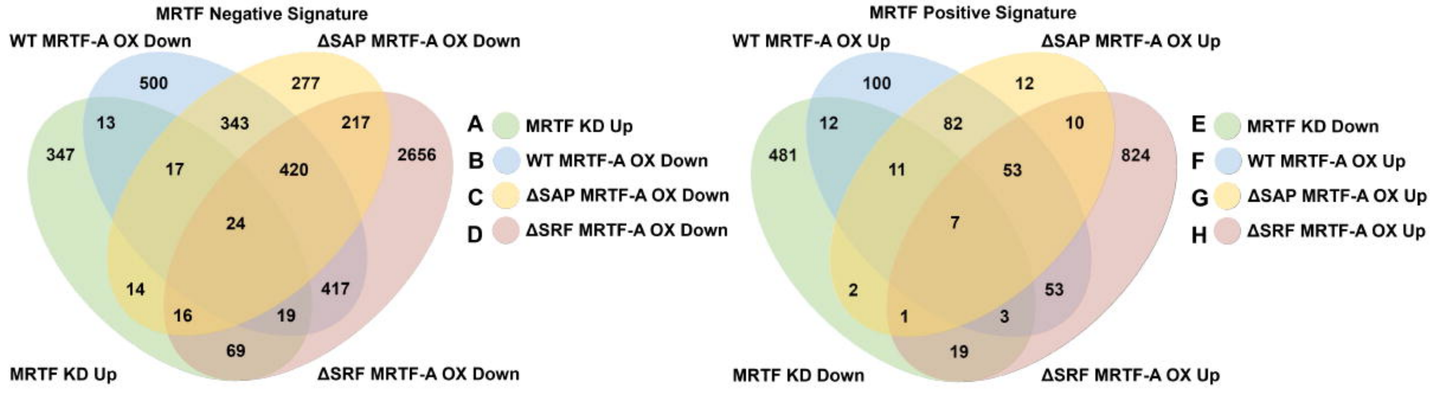

B

Definition	# of Genes	Interpretation
E&F	33	WT up-regulated genes
A&B	73	WT down-regulated genes
WT Up Score – WT Down Score		Difference in WT Scores
(E&F)-G	15	SAP-dependent up regulated genes
(A&B)-C	32	SAP-dependent down regulated genes
SAP Up Score – SAP Down Score		Difference in SAP Scores
(E&F)-H	23	SRF-dependent up regulated genes
(A&B)-D	30	SRF-dependent down regulated genes
SRF Up Score – SRF Down Score		Difference in SRF Scores

C

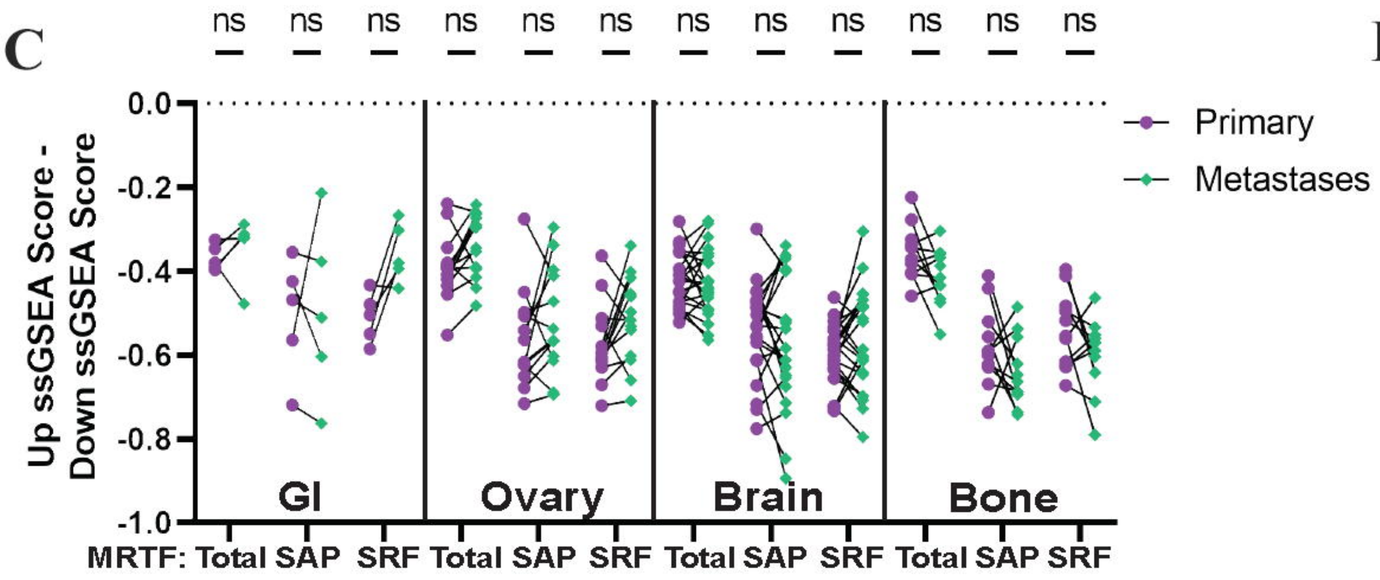
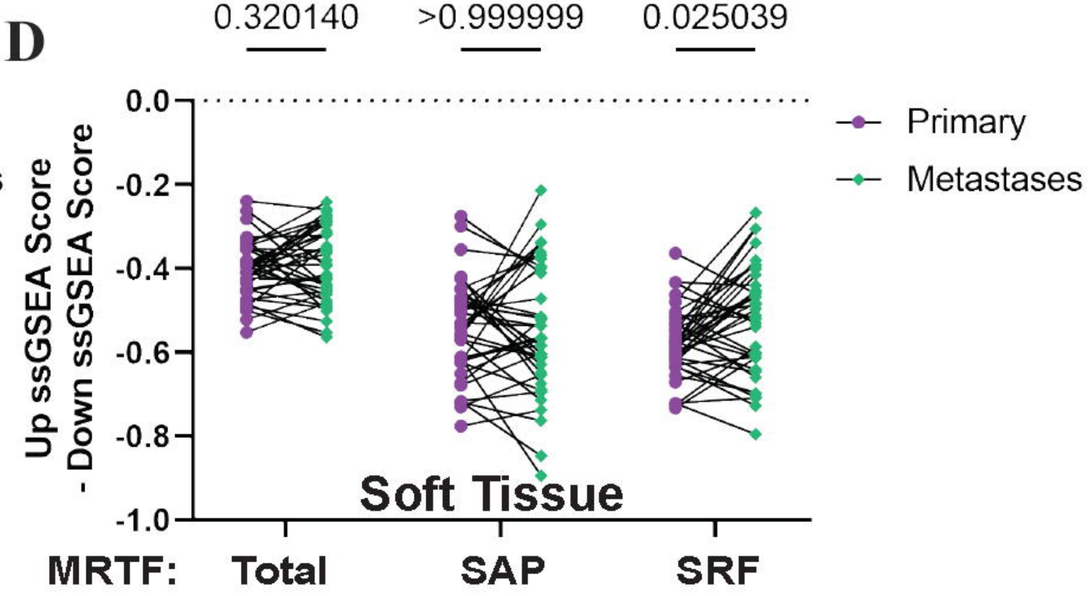
D